Electronic Supplementary Material (ESI) for Dalton Transactions.

Supplementary Information

Catalyst-Solvent Interactions in a Dinuclear Ru-Based Water Oxidation Catalyst

Andrey Shatskiy,[†] Reiner Lomoth,[‡] Ahmed F. Abdel-Magied,[†] Wangchuk Rabten,[†] Tanja M. Laine,[†] Hong Chen,[$,⊥] Junliang Sun,[$] Pher G. Andersson,[†] Markus D. Kärkäs,*[,†] Eric V. Johnston,*[,†] Björn Åkermark*[,†]

[†] Department of Organic Chemistry, Arrhenius Laboratory, Stockholm University, 10691 Stockholm, Sweden

[‡] Department of Chemistry, Ångström Laboratory, Uppsala University, 75120 Uppsala, Sweden

[$] Department of Materials and Environmental Chemistry, Stockholm University, 10691 Stockholm, Sweden

[⊥] Department of Chemistry, KTH Royal Institute of Technology, 10044 Stockholm, Sweden

E-mail: markus.karkas@su.se; eric.johnston@su.se; bjorn.akermark@su.se

1. Materials and Methods

1.1 General

All reagents were purchased from commercial suppliers and used without additional purification unless otherwise noted. HPLC grade organic solvents and MilliQ water (18.2 MΩ cm) were used for all experiments. Air-sensitive *m*-phenylenediamine was stored in a Schlenk tube under argon at −78 °C. $[Ru(DMSO)_4Cl_2]$,[S1] $[Ru(bpy)_2(bdc)](PF_6)_2$[S2] (where bpy = 2,2′-bipyridine, bdc = 4,4′-(dicarboxylic acid)-2,2′-bipyridine) and ruthenium complexes **1**[S3] and **2**[S4] were synthesized according to previously published procedures. The procedure for synthesis of compound **6** was adapted from reference [S5] and the procedure for formation of the dinuclear ruthenium complex **3** was adapted from reference [S6]. Flash chromatography was carried out with CombiFlash Rf 200 purification system using SiliCycle silicagel columns (12 or 25 g, 230–400 mesh 40–63 µm). ESI-MS was performed on Bruker Daltonics micrOTOF mass spectrometer. Elemental analysis was conducted by MEDAC Ltd (Chobham, UK). IR spectra were recorded on PerkinElmer Spectrum One FT-IR spectrometer.

1.2 NMR spectroscopy

^{1}H NMR and ^{13}C NMR spectra were recorded on a Bruker Ascend spectrometer at 400 and 100 MHz, respectively, or a Bruker Avance spectrometer at 500 MHz. ^{1}H NMR and ^{13}C NMR spectra were internally calibrated with residual undeuterated solvent peaks ($CDCl_3$: δ 7.26 for ^{1}H NMR and δ 77.16 for ^{13}C NMR; DMSO-d_6: δ 2.50 for ^{1}H NMR and δ 39.52 for ^{13}C NMR; CD_3OD: δ 3.31 for ^{1}H NMR and δ 49.00 for ^{13}C NMR; CD_3CN: δ 1.94 for ^{1}H NMR). Chemical shifts (δ) are reported in ppm and peak multiplicity is designated as s (singlet), d (doublet), t (triplet), m (multiplet), dd (doublet of doublets), and dt (doublet of triplets).

1.3 Electrochemical measurements

Electrochemical measurements were performed in a one-compartment three-electrode configuration cell connected to either a CH Instruments 750E bipotentiostat or an Autolab PGSTAT100 potentiostat. All solutions were deaerated with argon for at least 10 min before conducting the experiments and a slow flow of argon was maintained above the solutions during the experiments.

1.3.1 Electrochemical measurements in non-aqueous media

CH_2Cl_2 was dried on the VAC alumina drying column and then over activated 3 Å molecular sieves and used with tetrabutylammonium hexafluorophosphate ($TBAPF_6$, electrochemical grade, additionally dried in vacuum at 70 °C over P_2O_5) as supporting electrolyte (0.1 M). Glassy carbon disk (d = 3 mm) was used as a working electrode, platinum coil as a counter electrode, and a silver wire in a separate compartment (separated by a glass frit and filled with pure electrolyte solution) as a pseudo-reference electrode. A ferrocene solution (1 mM) in CH_2Cl_2 with $TBAPF_6$ (0.1 M) as supporting electrolyte was used as a standard to calibrate the pseudo-reference electrode before and after measurements on the solutions.

1.3.2 Electrochemical measurements in aqueous media

Electrochemical measurements in acidic aqueous media were conducted with addition of 10% MeCN in order to fully solubilize complex **3**. Triflic acid (0.1 M, pH 1.0) was used as supporting electrolyte with a 0.1 mM concentration of complex **3**. Glassy carbon disk (d = 1 mm) was used as a working electrode, glassy carbon rod as a counter electrode, and saturated calomel electrode (SCE) (separated from the analyte solution by a salt bridge) as a reference electrode. Positive feedback *iR*-compensation was used for cyclic voltammetry measurements at scan rates higher than 1 V s^{-1} with R = 150 Ω (determined by the circuit stability test).

Quantitative analysis of scan rate–dependent cyclic voltammetry data required subtraction of the background current. However, cyclic voltammograms obtained in the absence of complex **3** could not be used for the subtraction, presumably due to significant changes of the electric double layer properties caused by adsorption of complex **3**. Therefore, the background current was simulated by autofitting of experimental analyte cyclic voltammograms in the vicinity of the vertex potentials using OriginPro 8.0. The background fitting curves for anodic current were obtained using equation (S1), and the background fitting curves for the cathodic current were obtained using equation (S2), where i is current (A), E is potential (V), $p_{1–6}$ are adjustable fitting parameters, and p_7 is a fixed fitting parameter needed for setting of an appropriate initial fitting curve before the autofitting.

$$i = \{p_1 + p_2 \cdot E + p_3 \cdot \exp(p_4 \cdot E) + p_5 \cdot \exp(p_6 \cdot E)\} \cdot p_7 \quad \text{(S1)}$$

$$i = \{p_1 + p_2 \cdot E + p_5 \cdot \exp(p_6 \cdot E)\} \cdot p_7 \quad \text{(S2)}$$

Electrochemical measurements in neutral aqueous media were performed in phosphate buffer (0.1 M, pH 7.0) as supporting electrolyte with addition of 10% MeCN. Glassy carbon disk (d = 3 mm) was used as a working electrode, platinum coil as a counter electrode, and SCE as a reference electrode.

The Pourbaix diagram was constructed from the SWV data, which was recorded on 0.1 mM solution of complex **3** at varying pH. A Britton-Robinsson buffer (0.1 M) was used as supporting electrolyte and was adjusted to the desired pH by addition of aqueous NaOH (1.0 M) or H_2SO_4 (2.0 M), followed by addition of complex **3** in MeCN. Glassy carbon disk (d = 3 mm) was used as a working electrode, platinum coil as a counter electrode, and SCE as a reference electrode.

1.3.3 Determination of the surface concentration

The surface concentration of complex **3** on GC electrode was determined based on the CV data obtained with the aqueous TfOH solution of **3** (Figures S24 and S25). The background-subtracted voltammograms were fitted to theoretical model using equation (S3) (Figure S26),[S7] where Q is the charge passed through the electrode (C), w is the peak width, i is the current (A), v is the scan rate (V s^{-1}), E is the applied potential (V), and E_p is the peak potential (V). The fitting parameters Qv (peak area), E_p, and three independent w were adjusted for each peak and the obtained peak areas were used to determine the surface concentration according to equation (S4), where n is the number of transferred electrons, A is the electrode area (cm^2), and Γ is the surface concentration (mol cm^{-2}). The peak areas

displayed a linear dependence on the scan rate at $v \leq 20$ V s^{-1} with good charge balance between anodic and cathodic processes (Figure S26). Slopes of the linear fitting of the graphs at v = 0.5–20 V s^{-1} were then used to calculate the surface concentration of **3** to be ca. 5.7×10^{-11} mol cm^{-2}, which corresponds to 69% of a dense monolayer, assuming 2×10^{-14} cm^2 per molecule.

$$i = Qv\frac{3.53}{w}\frac{\exp\left\{\frac{3.53}{w}\left(E - E_{\mathrm{p}}\right)\right\}}{\left[1 + exp\left\{\frac{3.53}{w}\left(E - E_{\mathrm{p}}\right)\right\}\right]^2} \quad \text{(S3)}$$

$$Qv = nFA\Gamma v \quad \text{(S4)}$$

1.3.4 Determination of the rate constants from the forward-to-reverse peak current ratios

To confirm the values of the rate constants obtained from the analysis of scan rate dependent peak potentials the rate constants for reactions 2 and 3 were also determined from analysis of the forward-to-reverse peak current ratios. Equation (S5)[S8,S9] was numerically solved for the dimensionless kinetic parameter λ, which was then used to calculate the rate constants using equation (S6) and Figure S27, resulting in rate constants $k^{(2)}$ = 2×10^2 s^{-1} and $k^{(3)}$ = 4×10^1 s^{-1}.

$$\frac{i_{\mathrm{p,rev}}}{i_{\mathrm{p,fw}}} = \left\{1 + \exp\left[\frac{nF}{RT}\left(E_i - E_{1/2}\right)\right]\right\}^{-2\lambda}\left(\frac{1-\lambda}{2-\lambda}\right)^{2-\lambda}\left(\frac{2+\lambda}{1+\lambda}\right)^{2+\lambda} \quad \text{(S5)}$$

$$\lambda = \frac{kRT}{\nu nF} \quad \text{(S6)}$$

1.4 UV-vis spectroscopy

All UV-vis experiments were performed on Varian Cary 50 Bio UV-vis spectrometer using 1 or 10 mm quartz cuvettes. For the spectrophotometric redox titration of complex **3** (1 mm quartz cuvette) the stock solutions of CAN and **3** were prepared as follows: CAN was dissolved in an aqueous triflic acid (0.1 M, pH 1.0) to obtain a 5 mM stock solution; complex **3** was dissolved in MeCN to obtain a 1 mM stock solution. Thereafter, 0.1 mL of the stock solution of complex **3** was mixed with different amounts of aqueous triflic acid (0.1 M) and the CAN stock solution to obtain a set of 0.1 mM solutions of complex **3** (in 0.1 M triflic acid with 10% MeCN) containing 0–8 equiv. of CAN (with increments of 0.2 equiv.). Each solution was analysed within 2 min after preparation to exclude influence of slower reactions. In a similar manner, stock solution of **3** in MeCN was prepared for the spectrophotometric pH titration (10 mm quartz cuvette) and mixed with Britton-Robinsson buffer to obtain a 20 μM solution of **3** in Britton-Robinsson buffer with 10% MeCN. The pH of the buffer was adjusted by addition of aqueous NaOH (1.0 M) or H_2SO_4 (2.0 M).

1.5 On-line mass-spectrometry

On-line mass-spectrometry was used for monitoring of gaseous products produced during the water oxidation experiments catalyzed by complexes **1**, **2**, and **3**. The measurements were carried out on a custom-build mass-spectrometer equipped with MKS MicroVision Plus residual gas analyzer. For a detailed description of the setup see reference [S10]. During a typical catalytic run, a solution of catalyst of a desirable concentration in an appropriate solvent was prepared and deaerated with argon for 10 min. This solution was then injected into a sealed reaction chamber containing sacrificial oxidant ceric ammonium nitrate (CAN, ≥99.99% trace metals basis) under ca. 37 mbar of carrier gas (He). For the light-driven water oxidation, the photosensitizer ($[Ru(bpy)_2(bdc)](PF_6)_2$) and sacrificial electron acceptor ($Na_2S_2O_8$) were placed in the reaction chamber instead of CAN and a single blue LED (Creative Lighting Solutions, λ_{max} = 430–450 nm) was used as the light source. All catalytic experiments were performed at ambient temperature (ca. 23 °C) and in case of light-driven water oxidation a flow of pressurized air was used to maintain the temperature.

2. Synthetic Procedures and Analytical Data

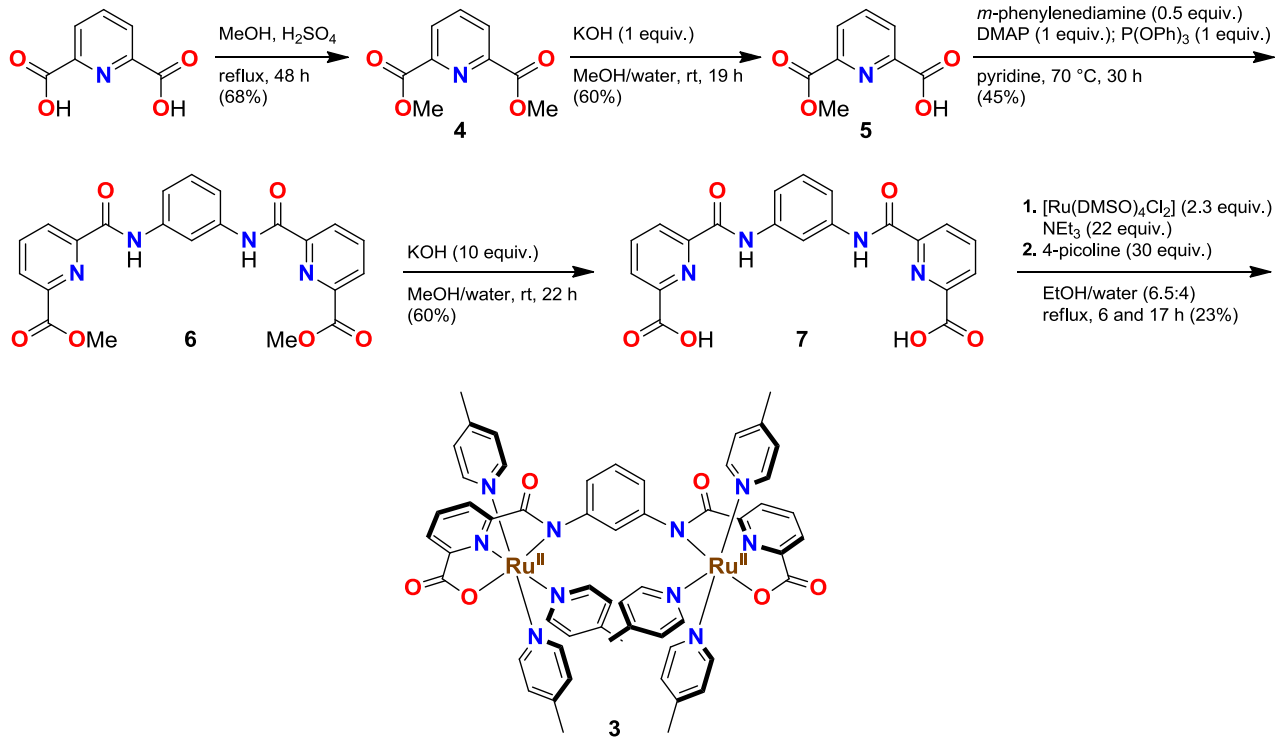

Scheme S1. Synthesis of the dinuclear ruthenium complex **3**.

Dimethyl 2,6-pyridinedicarboxylate (4): 2,6-pyridinedicarboxylic acid (12.0 g, 71.8 mmol) was dissolved in MeOH (200 mL) followed by dropwise addition of sulfuric acid (95–97%, 10 mL) under vigorous stirring. The reaction mixture was refluxed for 48 h and subsequently concentrated under reduced pressure. The residue was dissolved in CH_2Cl_2 (250 mL) and washed with 1.5 M solution of sodium hydroxide (3×80 mL). The organic layer was dried over anhydrous Na_2SO_4, filtered, concentrated under reduced pressure, and evacuated overnight, resulting in a yellowish crystalline product (9.5 g, 68%), which was used without further purification.

^{1}H NMR (400 MHz, $CDCl_3$): δ 8.30–8.29 (m, 1H), 8.29–8.27 (m, 1H), 8.03–7.97 (m, 1H), 3.99 (s, 6H).

^{13}C NMR (101 MHz, $CDCl_3$): δ 165.12, 148.30, 138.46, 128.11, 53.28.

ESI-MS (MeOH solution, positive mode): Calculated for $C_9H_{10}NO_4$ $[M + H]^+$: m/z 196.1, found: m/z 196.1.

Monomethyl 2,6-pyridinedicarboxylate (5): Ester **4** (8.86 g, 45.4 mmol) was mixed with 250 mL of methanol and heated until all solid material dissolved. Potassium hydroxide (2.55 g, 45.4 mmol, 1 equiv.) was added as a solution in minimum amount of water and the reaction mixture was stirred at room temperature. After 19 h the reaction mixture was concentrated under reduced pressure, resulting in a white solid. The solid was dissolved in 200 mL of water and washed with CH_2Cl_2 (2×25 mL). The aqueous layer was acidified with 46 mL of 1 M hydrochloric acid and the desirable product was extracted with ethyl acetate (5×50 mL). The combined organic phases were dried over anhydrous Na_2SO_4, filtered, concentrated under reduced pressure, and evacuated overnight, resulting in a white crystalline product (4.9 g, 60%), which was used without further purification.

^{1}H NMR (400 MHz, $CDCl_3$): δ 8.42 (dd, J = 7.7, 1.1 Hz, 1H), 8.36 (dd, J = 7.8, 1.1 Hz, 1H), 8.13 (t, J = 7.8 Hz, 1H), 4.04 (s, 3H).

^{13}C NMR (101 MHz, $CDCl_3$): δ 164.28, 163.63, 146.92, 146.53, 139.79, 128.93, 126.96, 53.33.

ESI-MS (MeOH solution, positive mode): Calculated for $C_8H_7NNaO_4$ $[M + Na]^+$: m/z 204.0, found: m/z 204.0.

Dimethyl 6,6'-((1,3-phenylenebis(azanediyl))bis(carbonyl))dipicolinate (6): Monoester **5** (3.00 g, 16.6 mmol), *m*-phenylenediamine (0.896 g, 8.28 mmol, 0.5 equiv.), and 4-dimethylaminopyridine (DMAP, 2.02 g, 16.6 mmol, 1 equiv.) were mixed and deaerated by evacuation and backfilling with nitrogen gas (3x). Deaerated pyridine (75 mL, dried over 3 Å molecular sieves) was added to the solids and the reaction mixture was stirred for 15 min, followed by addition of triphenyl phosphite (4.30 mL, 16.6 mmol, 1 equiv.), after which the resulting yellow suspension was stirred at 70 °C under nitrogen. During the course of the reaction the reaction mixture turned into a transparent yellow solution. After 30 h the reaction mixture was concentrated under reduced pressure. The yellow oily residue was mixed with water and formed a white precipitate upon vigorous shaking. The precipitate was transferred to a glass filter and extensively washed with water and Et_2O, resulting in a white solid. The crude product

was purified by automated flash chromatography on silica column (CH_2Cl_2/EtOAc, 0% to 30% gradient of EtOAc) and the product fractions were combined, concentrated under reduced pressure, and evacuated overnight, resulting in the title compound as a white solid (1.61 g, 45%).

^{1}H NMR (400 MHz, $CDCl_3$): δ 10.05 (s, 2H), 8.51 (dd, J = 7.8, 1.2 Hz, 2H), 8.32–8.27 (m, 3H), 8.08 (t, J = 7.8 Hz, 2H), 7.67 (dd, J = 8.1, 2.1 Hz, 2H), 7.44 (t, J = 8.1 Hz, 1H), 4.07 (s, 6H).

^{13}C NMR (101 MHz, $CDCl_3$): δ 165.05, 161.51, 150.15, 146.78, 139.01, 138.26, 129.89, 127.73, 125.76, 116.56, 111.85, 53.18.

ESI-MS (MeOH solution, positive mode): Calculated for $C_{22}H_{19}N_4O_6$ $[M + H]^+$: m/z 435.1, found: m/z 435.1.

6,6'-((1,3-phenylenebis(azanediyl))bis(carbonyl))dipicolinic acid (7): Diester **6** (1.34 g, 3.07 mmol) was suspended in MeOH (60 mL) followed by addition of KOH (1.73 g, 30.7 mmol, 10 equiv.) dissolved in minimum amount of water and the reaction mixture was stirred at room temperature. After 22 h the reaction mixture was concentrated under reduced pressure, resulting in a bright yellow solid. The solid was dissolved in 100 mL of water, forming a colorless transparent solution. The solution was washed with CH_2Cl_2 (2×20 mL) and the aqueous layer was acidified to pH 6 with HCl (31.4 mL, 1.0 M, 1 equiv. relative to KOH). A white precipitate was formed upon addition of acid. The precipitate was suspended and divided into four 50 mL falcon tubes and centrifuged (4100 rpm, 10 min). The supernatant was decanted and the residual solid was washed with water and centrifuged (3×40 mL for each falcon tube). The combined solids were dried over P_2O_5 for two days, resulting in the title compound as a white solid (0.74 g, 60%), which was used without further purification.

^{1}H NMR (400 MHz, DMSO-d_6): δ 13.31 (s, 2H), 10.94 (s, 2H), 8.43 (dd, J = 7.2, 1.6 Hz, 3H), 8.37–8.26 (m, 4H), 7.67 (dd, J = 8.1, 1.8 Hz, 2H), 7.48 (t, J = 8.1 Hz, 1H).

^{13}C NMR (101 MHz, DMSO-d_6): δ 164.73, 161.45, 149.08, 146.14, 140.26, 138.39, 129.23, 127.08, 125.89, 116.61, 112.90.

ESI-MS (MeOH solution, positive mode): Calculated for $C_{20}H_{14}N_4NaO_6$ $[M + Na]^+$: m/z 429.1, found: m/z 429.1.

Dinuclear ruthenium complex (3): Ligand **7** (0.53 g, 1.30 mmol) was suspended in a mixture of EtOH (50 mL) and water (80 mL) followed by addition of Et_3N (4.0 mL, 28.6 mmol, 22.0 equiv.) and heating to the boiling point, which resulted in a colorless solution. The solution was deaerated with nitrogen gas for 15 min. In a separate flask, $[Ru(DMSO)_4Cl_2]$ (1.45 g, 3.00 mmol, 2.30 equiv.) was mixed with EtOH (80 mL), the mixture was deaerated with nitrogen for 15 min and then heated to reflux, resulting in a homogeneous yellow solution. The solution of the deprotonated ligand **7** was added to the refluxing $[Ru(DMSO)_4Cl_2]$ solution with a syringe pump over 5 h, upon which the solution became dark red. After the addition was finished the reaction mixture was refluxed for an additional hour, 4-picoline (3.80 mL, 39.1 mmol, 30.0 equiv.) was added, and the resulting solution

was refluxed for additional 17 h. The reaction mixture was concentrated under reduced pressure, resulting in a dark-brown solid, which was placed in a falcon tube and washed with water (1×40 mL, 2×20 mL), acetone (2×15 mL), and Et_2O (2×15 mL) using centrifuge (4100 rpm, 10 min). The filter was then evacuated overnight, resulting in a brown solid (0.47 g). The crude product was purified by automated flash chromatography on silica column (CH_2Cl_2/MeOH, 0% to 10% gradient of MeOH). The fractions containing the desirable product were combined, concentrated under reduced pressure, and evacuated for two days, resulting in complex **3** as a dark brown solid (0.35 g, 23%).

^{1}H NMR (500 MHz, CD_3OD with 6 equiv. of ascorbic acid): δ 8.35–8.30 (m, 4H), 8.08 (dd, J = 7.6, 1.5 Hz, 2H), 7.82–7.73 (m, 12H), 7.25 (dt, J = 5.4, 0.9 Hz, 4H), 7.15 (t, J = 7.9 Hz, 1H), 6.82 (dd, J = 7.9, 2.0 Hz, 2H), 6.77 (dt, J = 5.6, 0.9 Hz, 8H), 6.23 (t, J = 2.0 Hz, 1H), 2.38 (s, 6H), 2.19 (s, 12H).

^{13}C NMR (101 MHz, CD_3OD with 6 equiv. of ascorbic acid): δ 175.34, 172.27, 160.38, 155.12, 154.14, 151.30, 149.86, 132.95, 127.56, 127.23, 126.93, 126.44, 123.31, 20.85, 20.62.

ESI-MS (MeOH solution, positive mode): Calculated for $C_{56}H_{52}N_{10}O_6Ru_2$ $[M]^+$ (see Figure S16 for isotope pattern): m/z 1164.2, found: m/z 1164.2.

Elemental analysis. Found: C 54.92; H 4.67; N 11.07; Cl 0.76; Ru 15.30. Calculated for $C_{56}H_{52}N_{10}O_6Ru_2 \cdot 0.13CH_2Cl_2 \cdot 3H_2O$: C 54.89; H 4.78; N 11.40; Cl 0.75; Ru 16.46.

IR (KBr disk, cm^{-1}) ν_{max} = 3431, 3231, 1638, 1617, 1594, 1560, 1498, 1474, 1385, 1341, 1208, 1177, 1040, 815, 785, 766, 721, 688, 508.

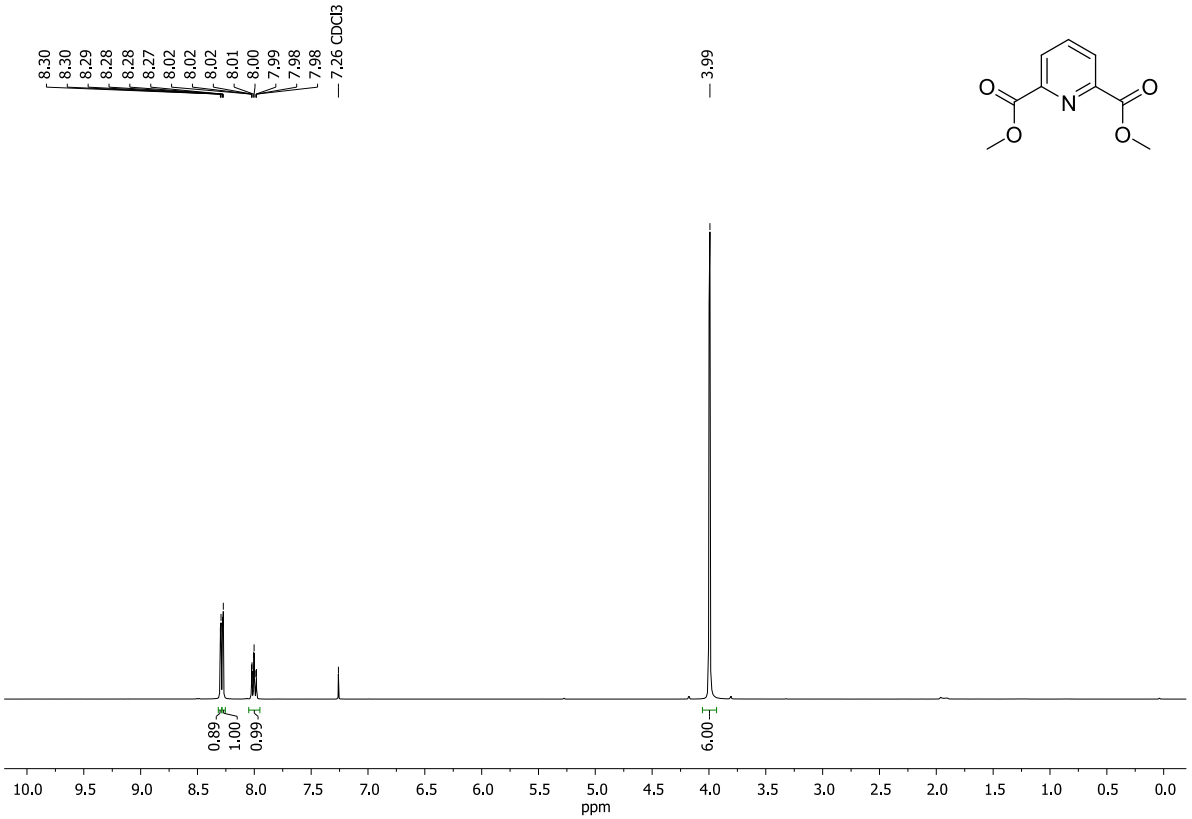

Figure S1. ^{1}H NMR spectrum of diester **4** in $CDCl_3$.

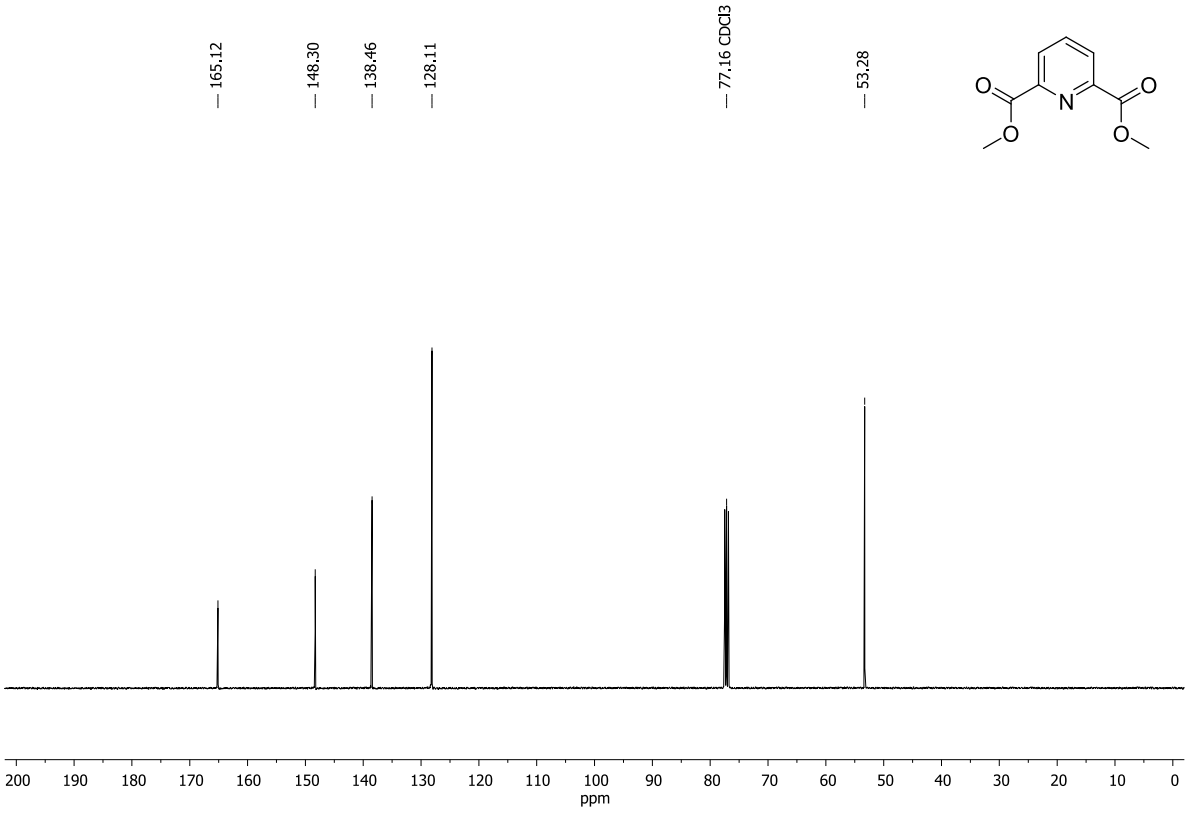

Figure S2. ^{13}C NMR spectrum of diester **4** in $CDCl_3$.

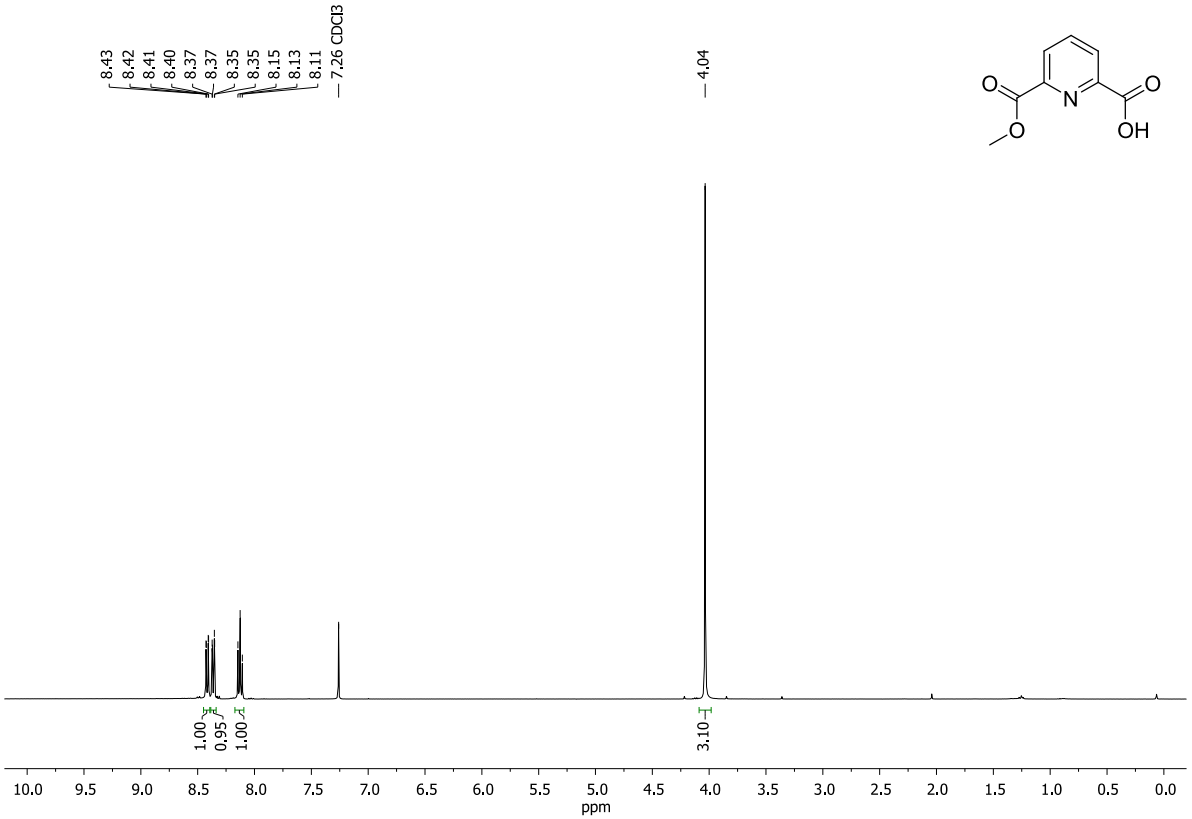

Figure S3. ^{1}H NMR spectrum of monoester **5** in $CDCl_3$.

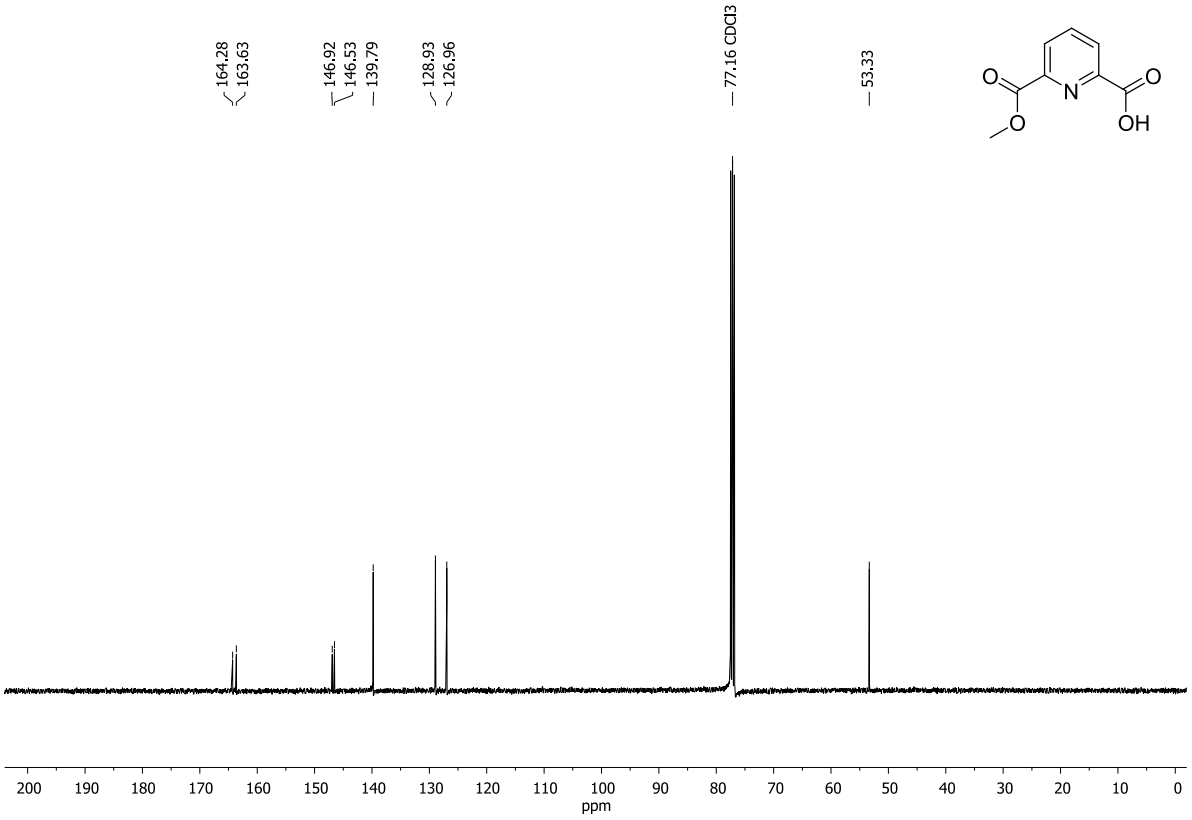

Figure S4. ^{13}C NMR spectrum of monoester **5** in $CDCl_3$.

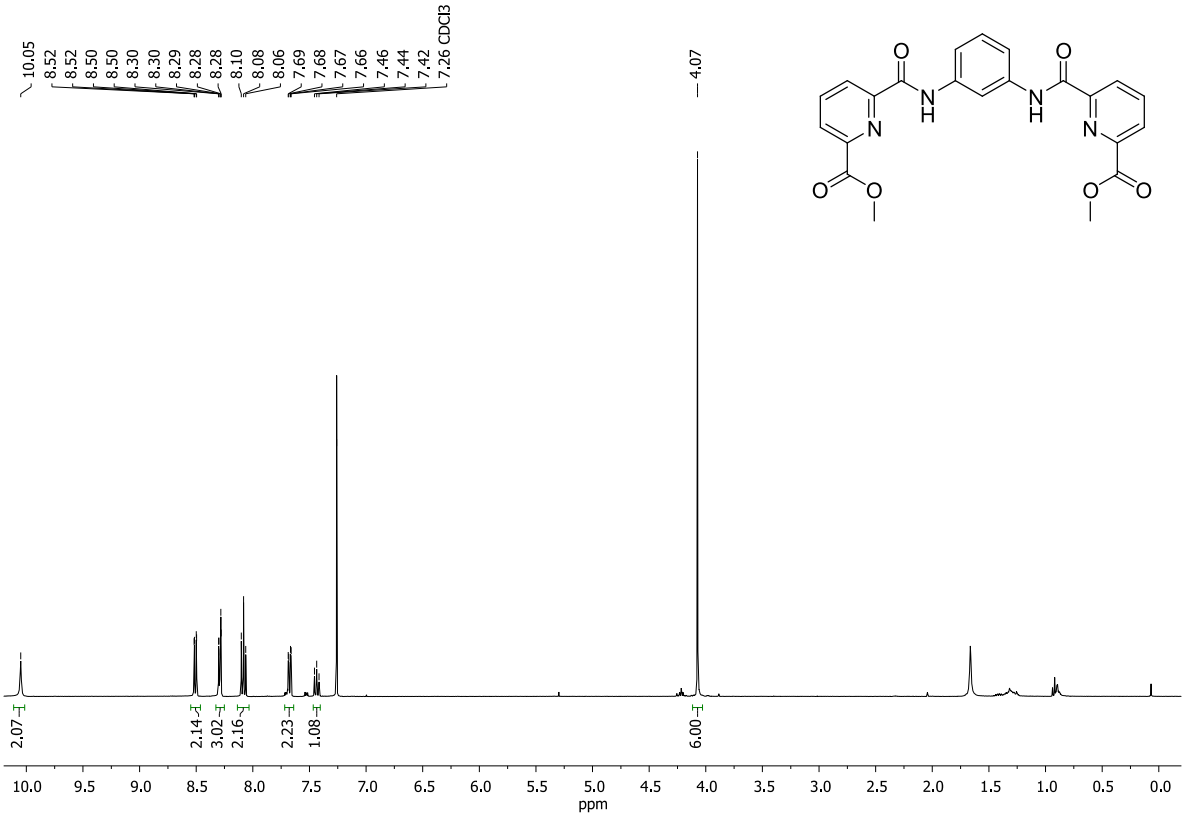

Figure S5. ^{1}H NMR spectrum of diester **6** in $CDCl_3$.

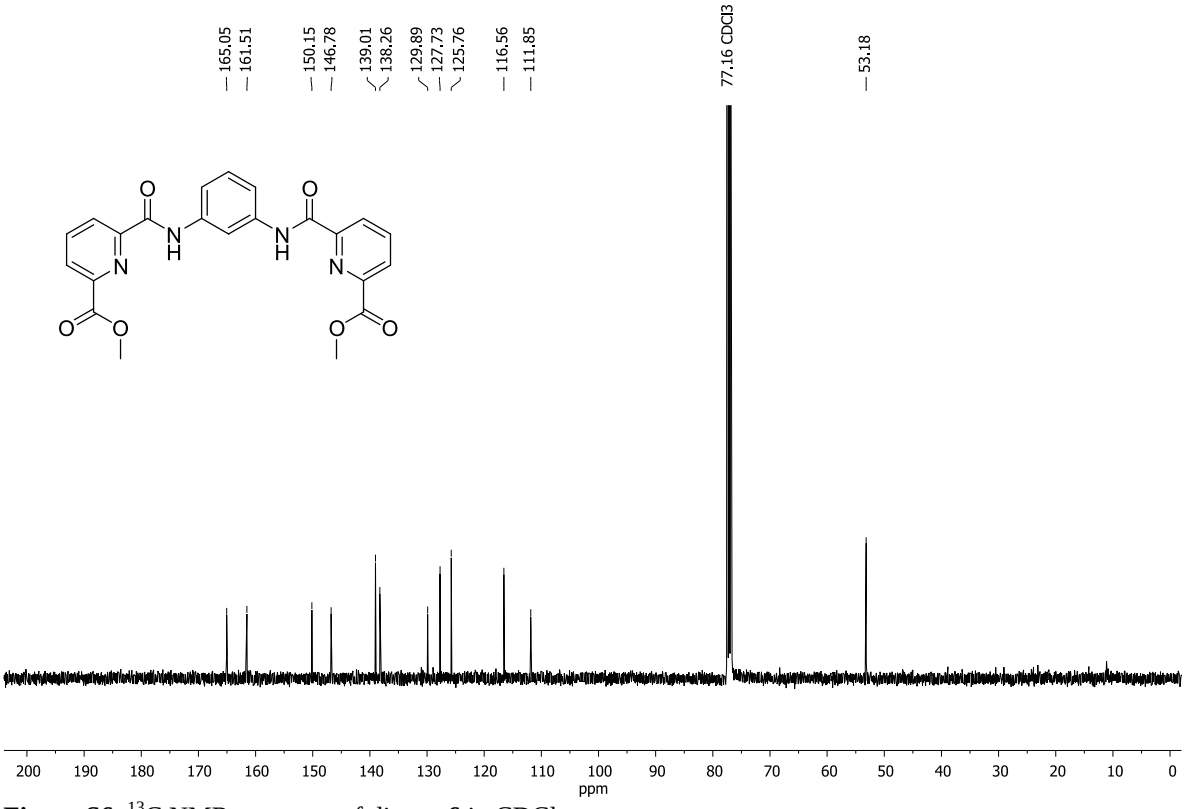

Figure S6. ^{13}C NMR spectrum of diester **6** in $CDCl_3$.

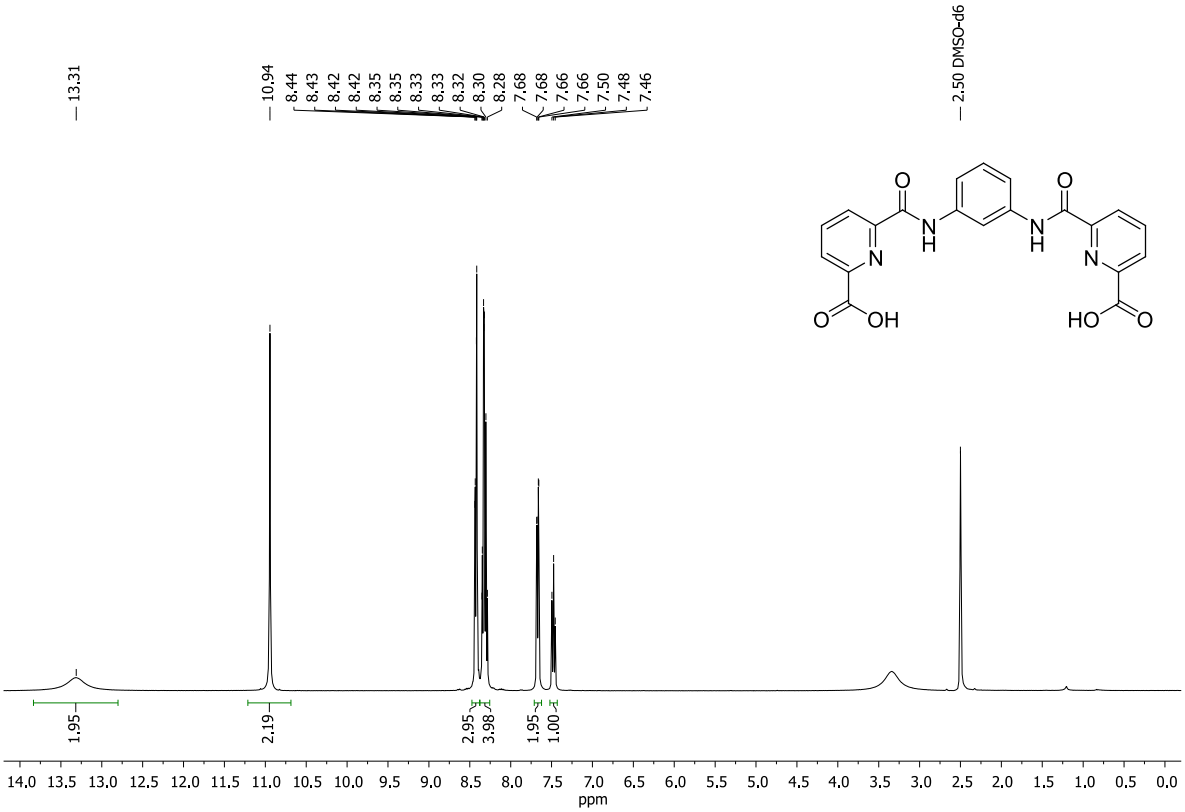

Figure S7. ^{1}H NMR spectrum of ligand **7** in DMSO-d_6.

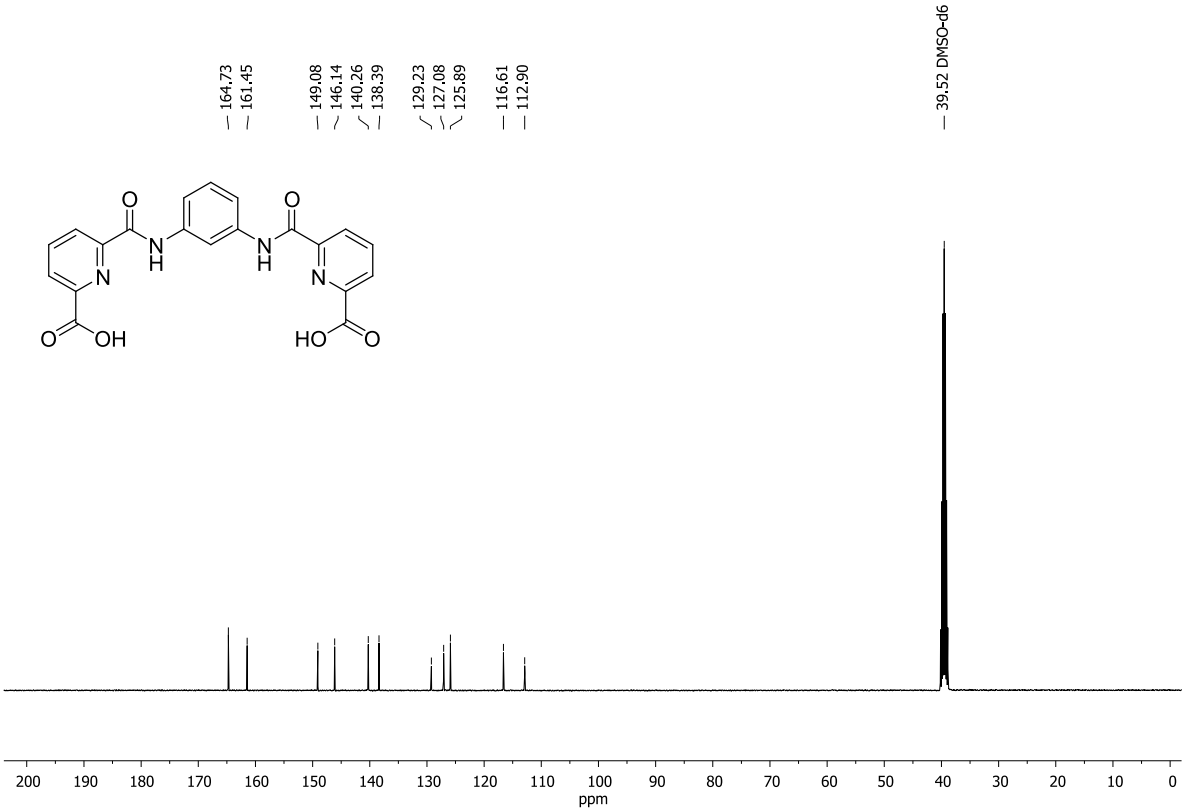

Figure S8. ^{13}C NMR spectrum of ligand **7** in DMSO-d_6.

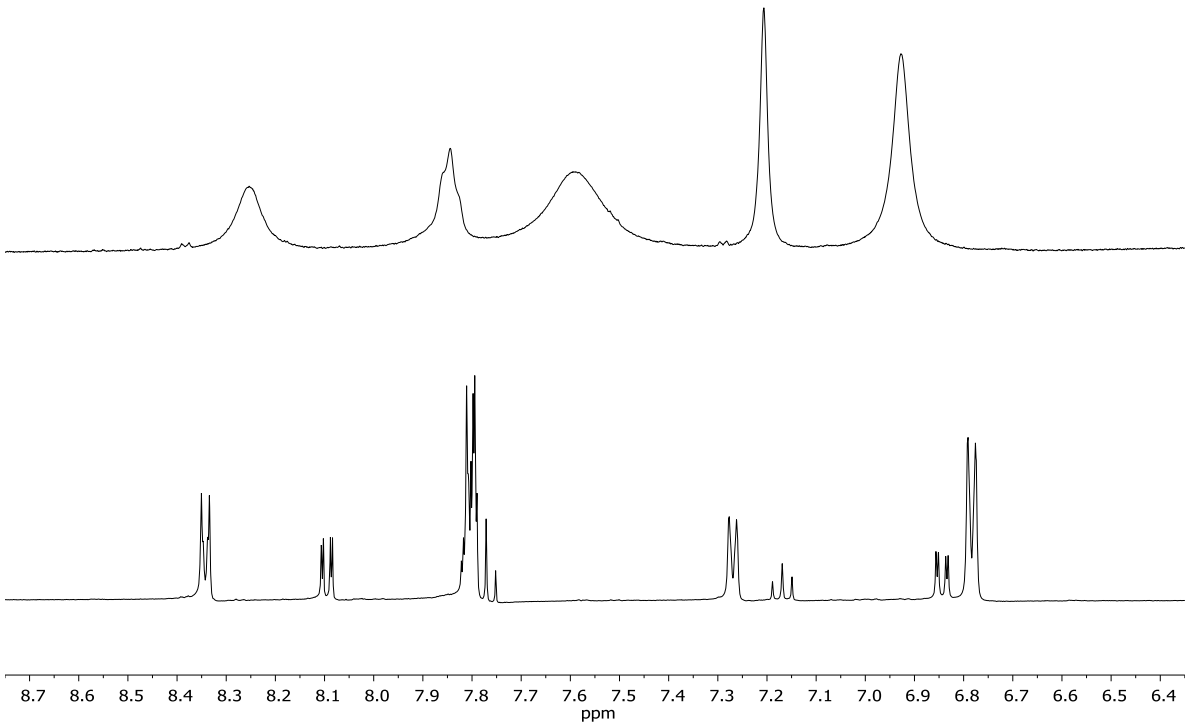

Figure S9. Aromatic region of the ^{1}H NMR spectrum of complex **3** in CD_3OD (5 mM) before (top) and after (bottom) addition of 0.05 equiv. of ascorbic acid.

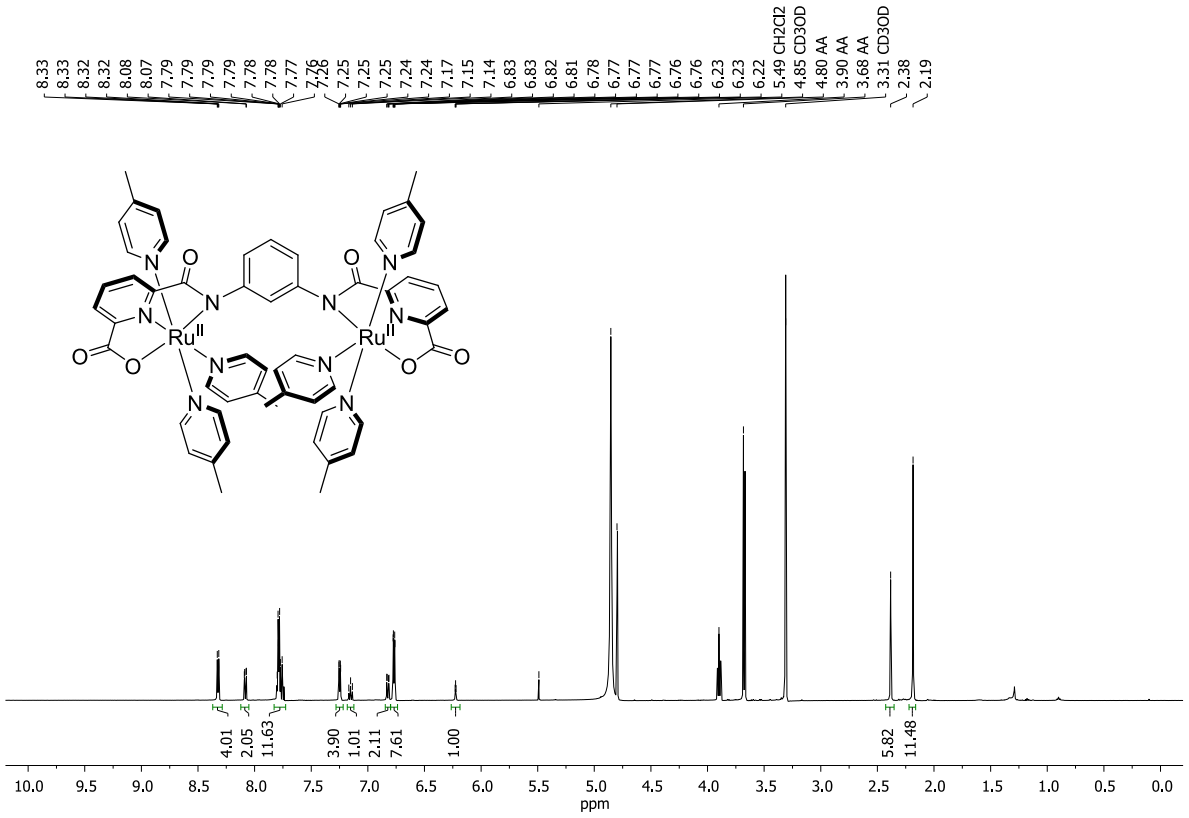

Figure S10. ^{1}H NMR spectrum of complex **3** in CD_3OD (5 mM) after addition of excess (ca. 6 equiv.) ascorbic acid.

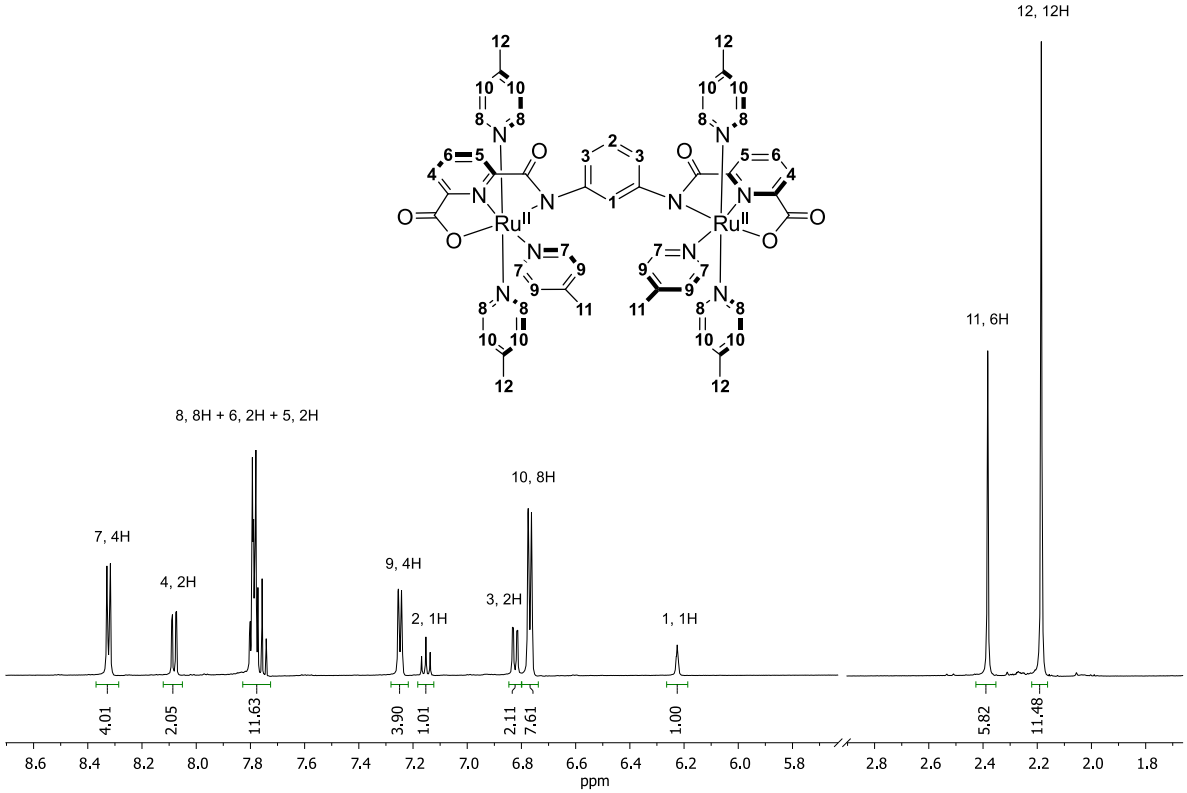

Figure S11. Assignment of ^{1}H NMR spectrum of complex **3** in CD_3OD (5 mM) after addition of excess (ca. 6 equiv.) ascorbic acid.

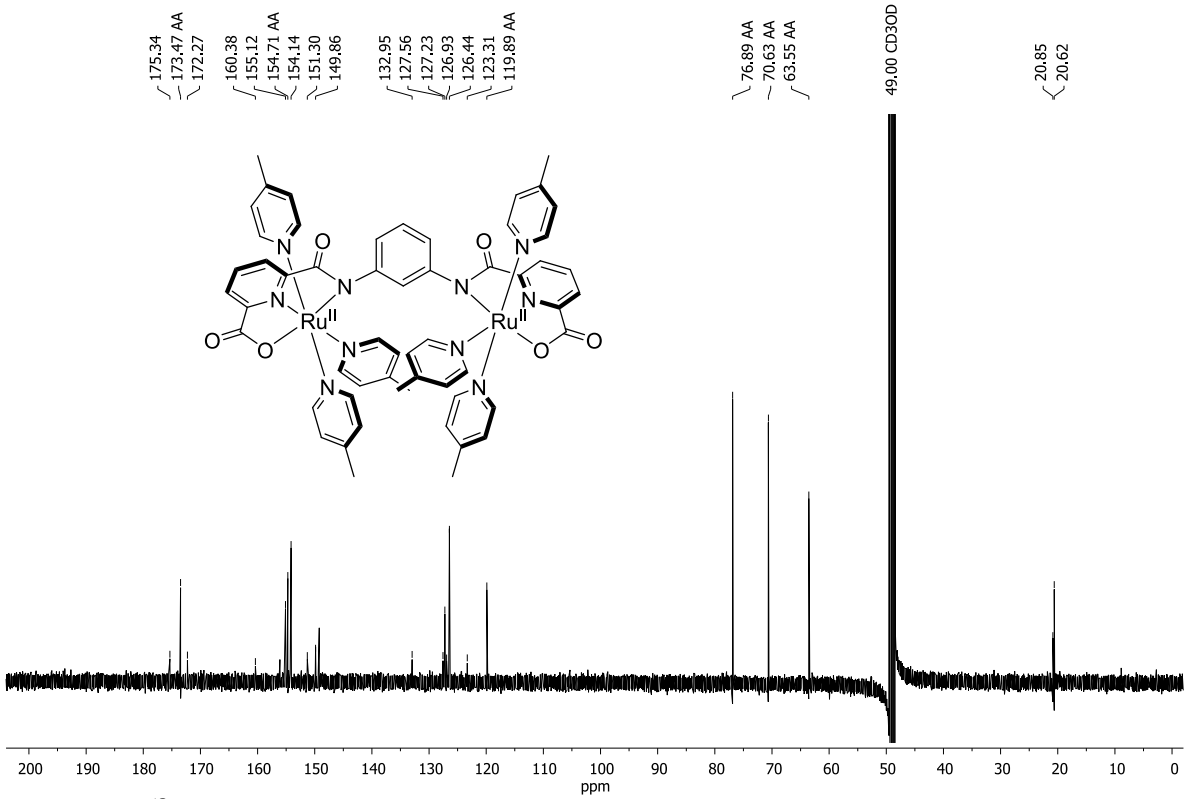

Figure S12. ^{13}C NMR spectrum of complex **3** in CD_3OD (5 mM) with addition of excess (ca. 6 equiv.) ascorbic acid.

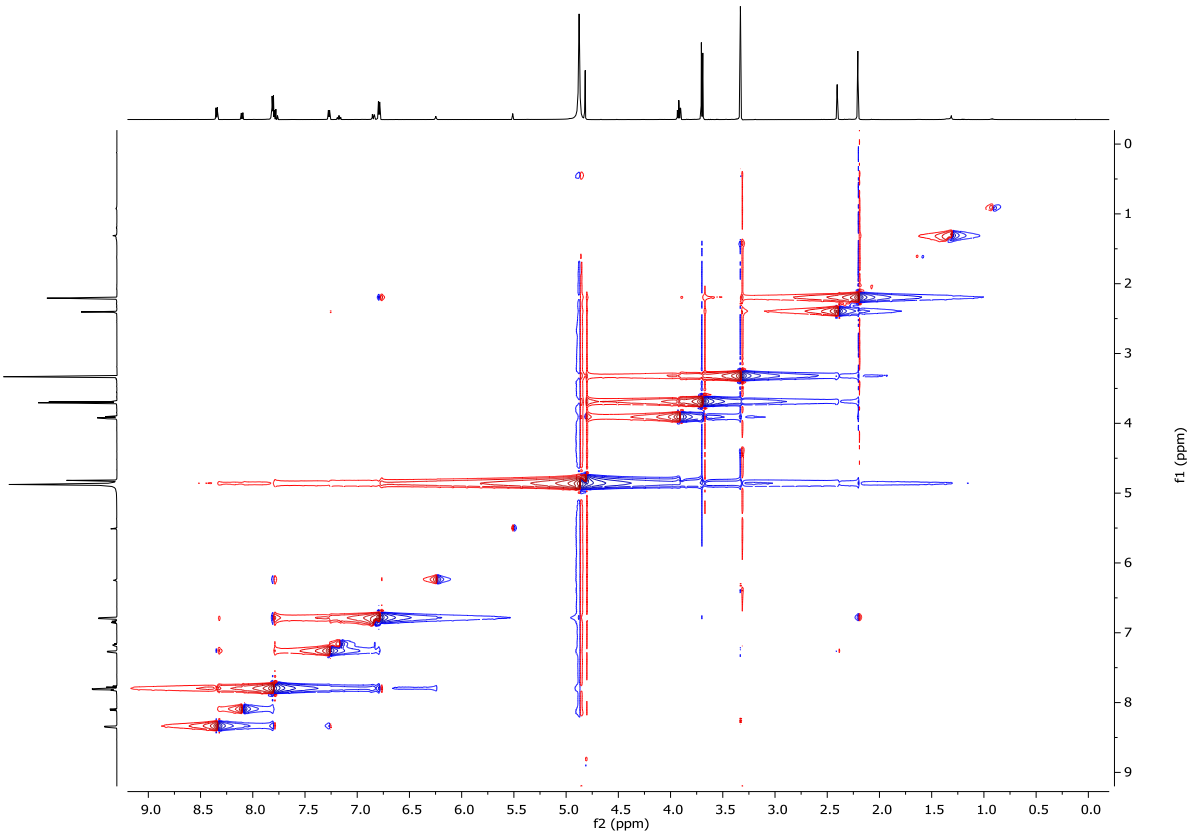

Figure S13. NOESY NMR of complex **3** in CD_3OD (5 mM) after addition of excess (ca. 6 equiv.) ascorbic acid.

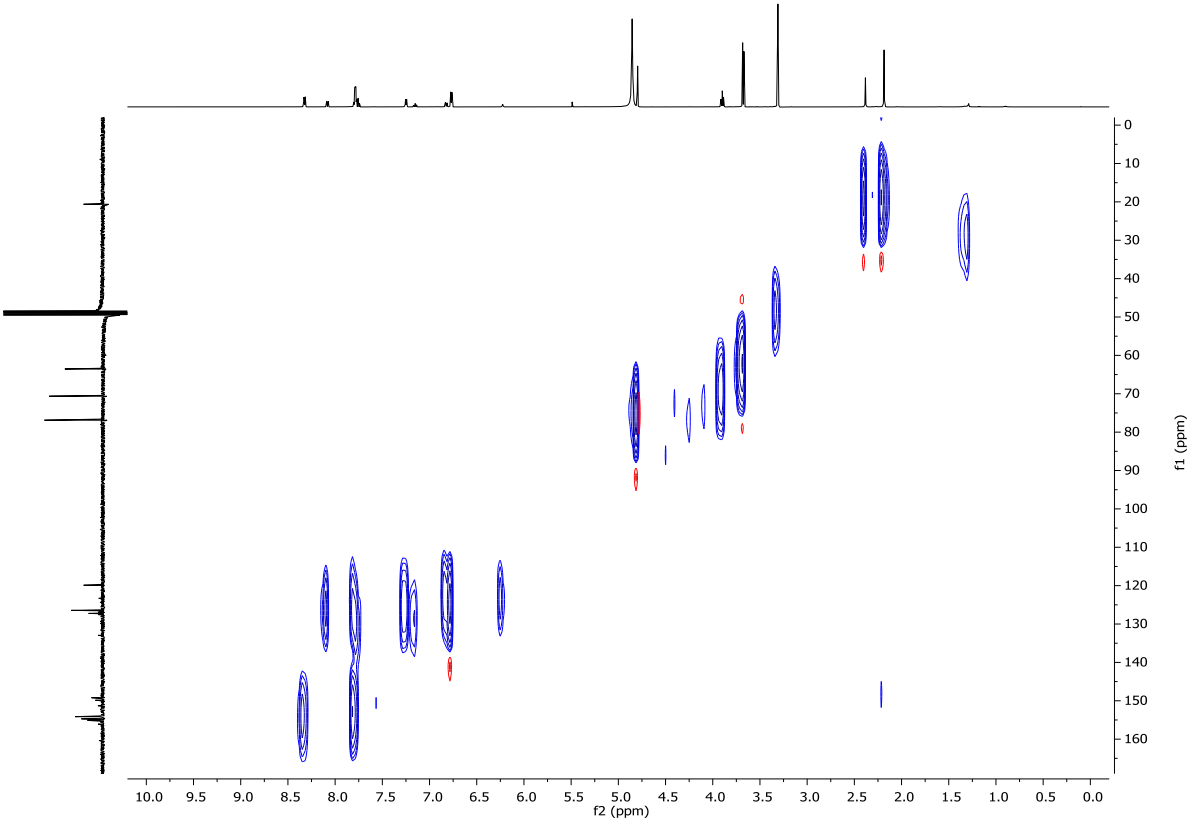

Figure S14.HSQC NMR of complex **3** in CD_3OD (5 mM) after addition of excess (ca. 6 equiv.) ascorbic acid.

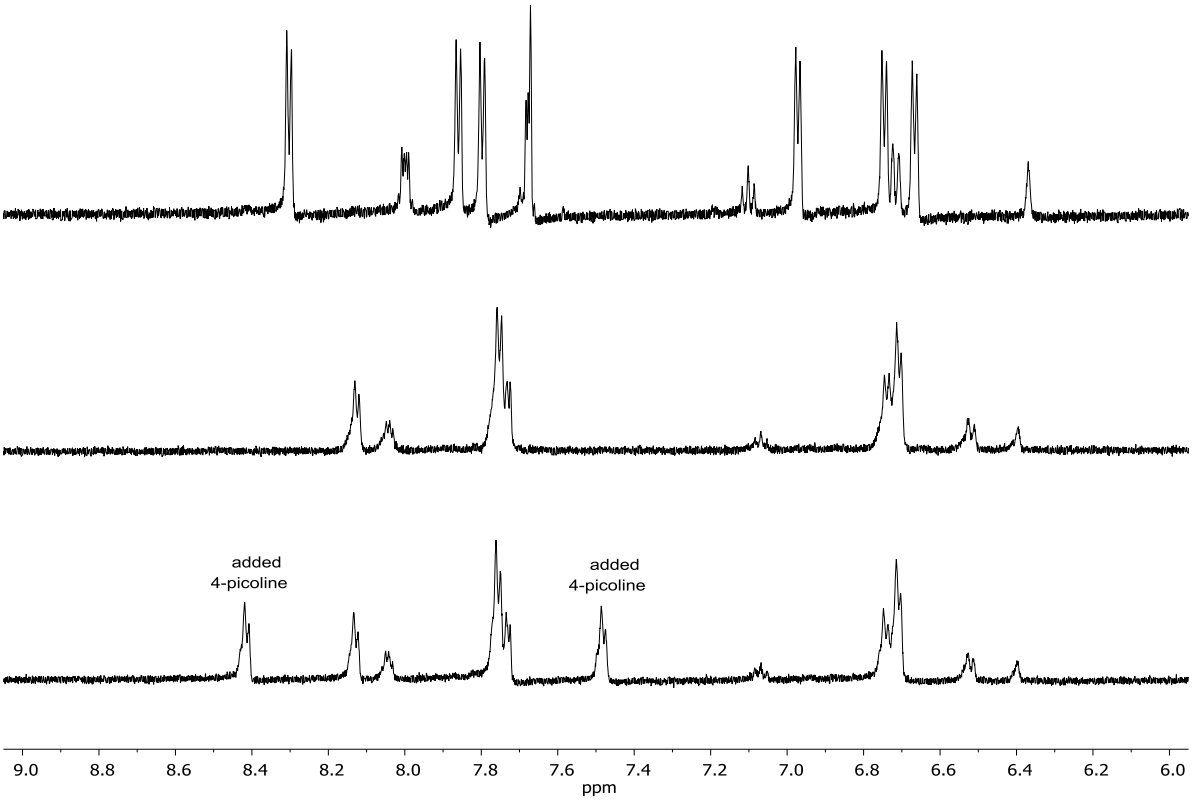

Figure S15. Aromatic region of the ^{1}H NMR spectrum of complex **3** (1 mM) after addition of excess (ca. 6 equiv.) ascorbic acid in: CD_3CN (top); CD_3CN/D_2O 3:1 (middle); and CD_3CN/D_2O 3:1 with addition of 2 equiv. of 4-picoline (bottom).

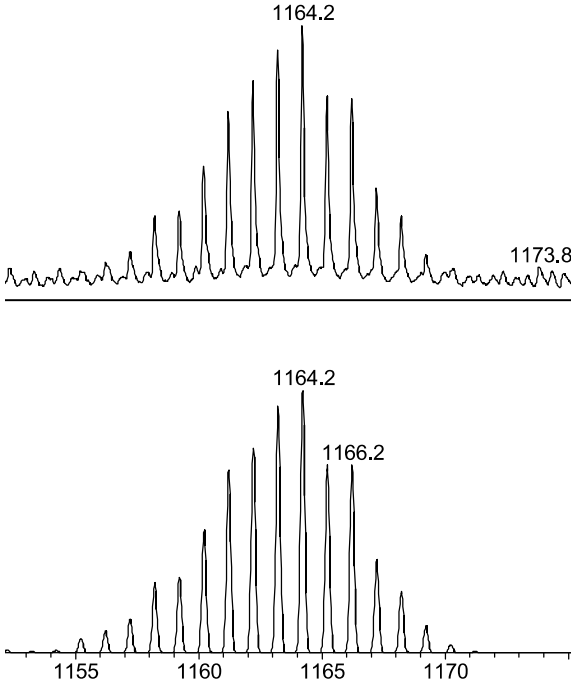

Figure S16. ESI-MS peak of the molecular ion of complex **3** recorded in positive mode. 0.5 µg/mL solution of complex **3** in MeOH (top), and simulated mass-spectrum of $[C_{56}H_{52}N_{10}O_6Ru_2]^+$ (bottom).

Table S1. Relevant bond lengths and angles for dinuclear ruthenium complex **3** and mononuclear ruthenium complex **2**.[a] See Section 4 for details on the crystal structure of complex **3**.

Bond between atoms:	Bond length (Å)		Angle between atoms:	Angle (deg)	
	3	**2**[S11]		**3**	**2**[S11]
Ru–N, equatorial pyridine	1.952(4) 1.948(4)	1.958(3)	N–Ru–N, backbone pyridine to carboxamide	78.28 78.53	79.60
Ru–N, carboxamide	2.110(4) 2.122(4)	2.024(3)	N–Ru–O, backbone pyridine to carboxylate	79.53 79.48	80.44
Ru–O, carboxylate	2.141(4) 2.135(4)	2.043(3)	N–Ru–N, backbone pyridine to equatorial picolins	176.76 175.69	178.07
Ru–N, axial picolines	2.108(5) 2.101(5)	2.087(3)	N–Ru–N, backbone pyridine to axial picolines	91.58 & 93.51 88.84 & 88.52	91.10 90.52
	2.118(5) 2.087(4)	2.095(3)	N–Ru–N, axial picolines	174.36 177.37	176.77
Ru–N, equatorial picolines	2.132(4) 2.127(4)	2.108(3)	N–Ru–O, carboxamide and carboxylate	157.78 157.97	160.00

[a] the bond lengths and angles are presented in pairs for two catalytic units of complex **3**

3. Electrochemistry and UV-vis Spectroscopy Data

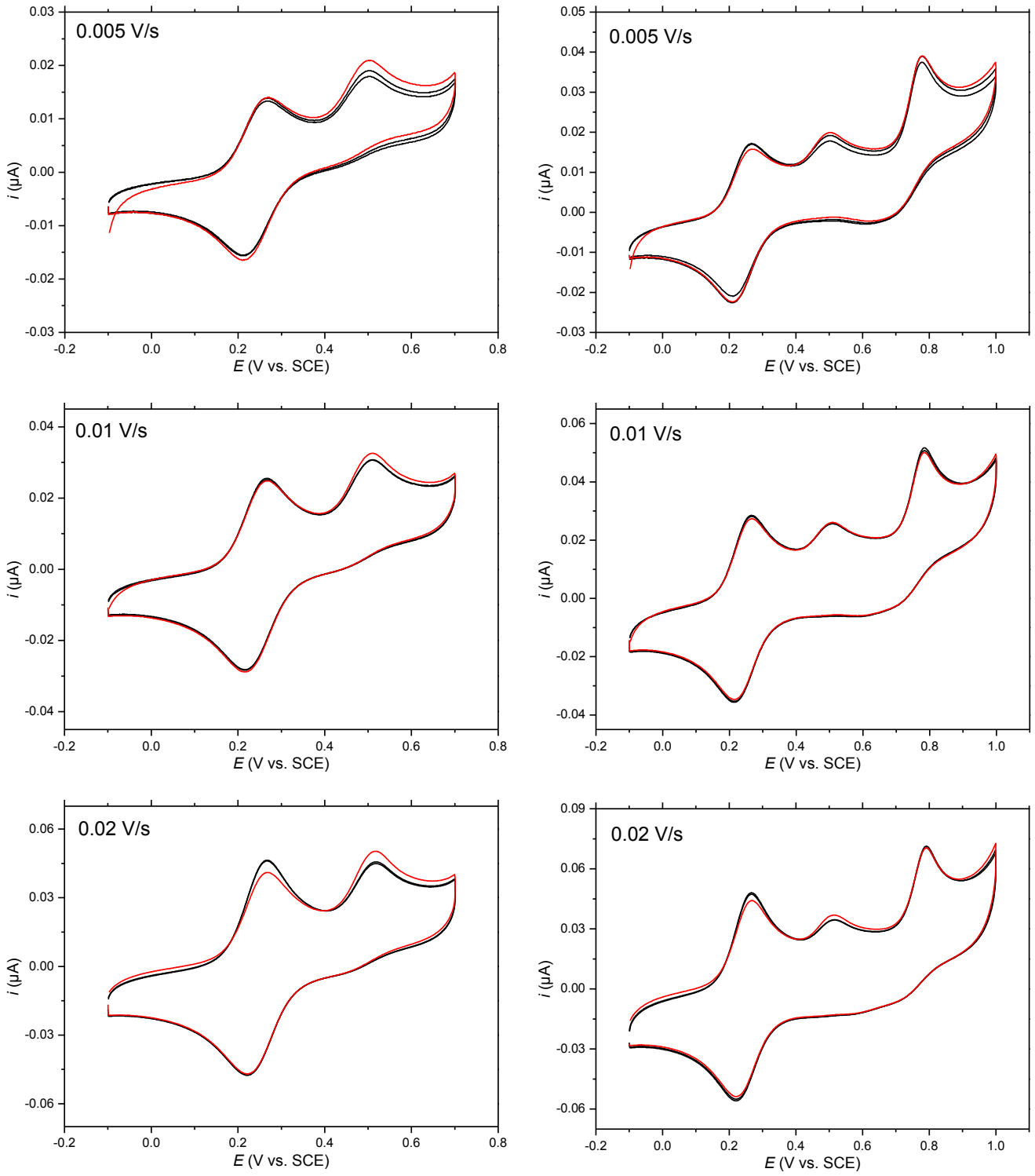

Figure S17. Cyclic voltammograms of complex **3** in aqueous TfOH at scan rates 0.005, 0.01, and 0.02 V/s. The first scan (red) and two consecutive (black) scans are shown. For details see Section 1.3.2.

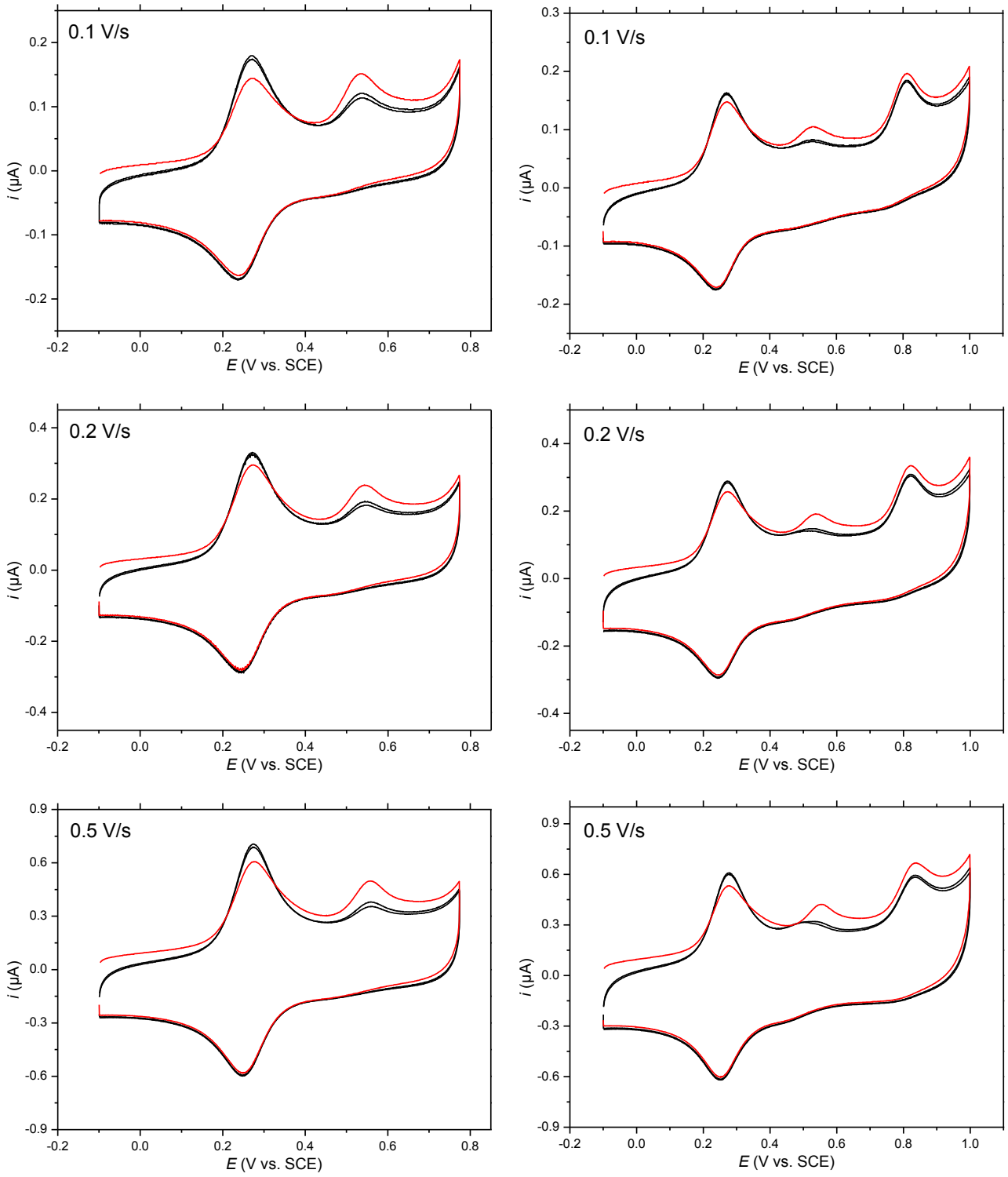

Figure S18. Cyclic voltammograms of complex **3** in aqueous TfOH at scan rates 0.1, 0.2, and 0.5 V/s. The first scan (red) and two consecutive (black) scans are shown. For details see Section 1.3.2.

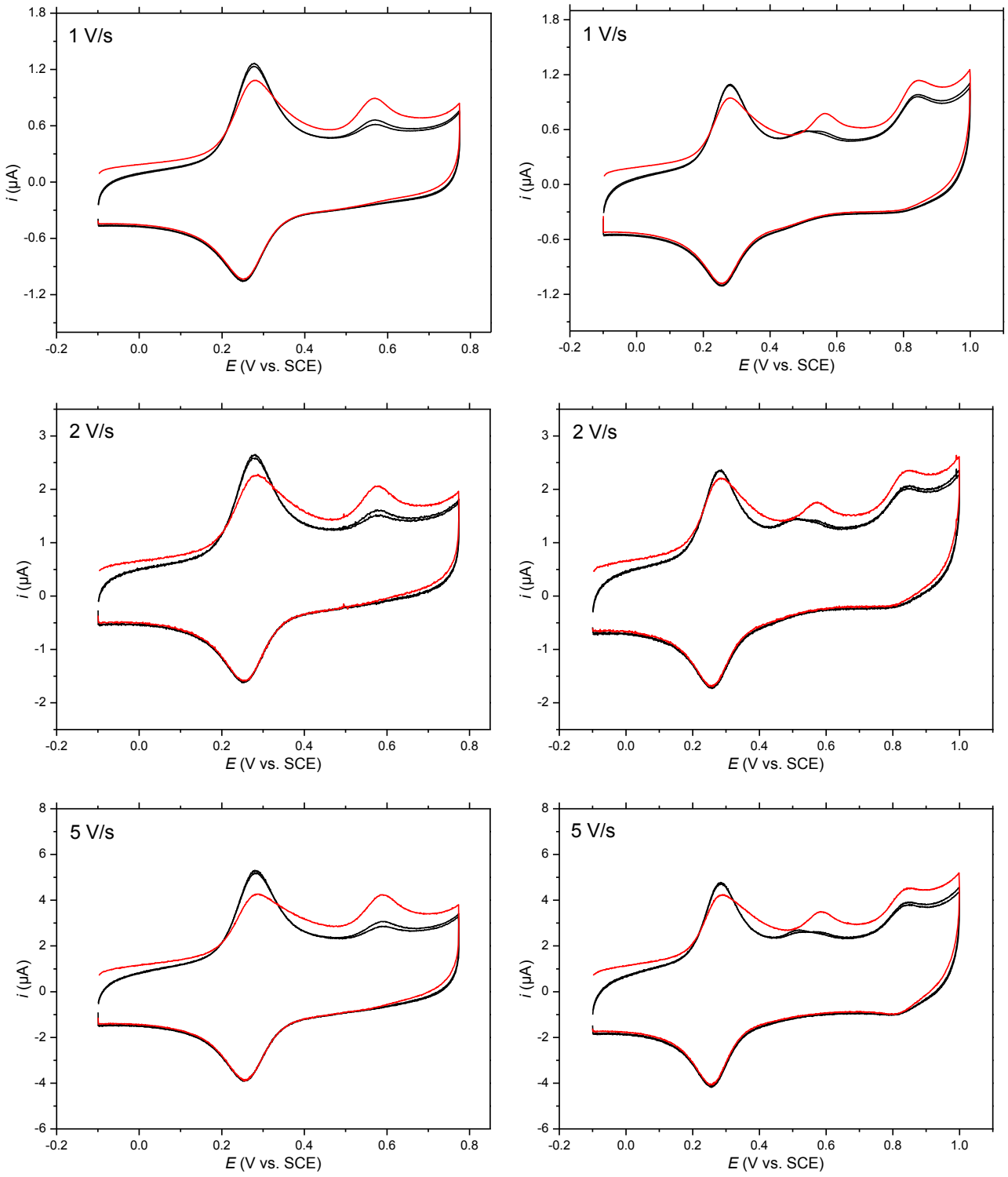

Figure S19. Cyclic voltammograms of complex **3** in aqueous TfOH at scan rates 1, 2, and 5 V/s. The first scan (red) and two consecutive (black) scans are shown. For details see Section 1.3.2.

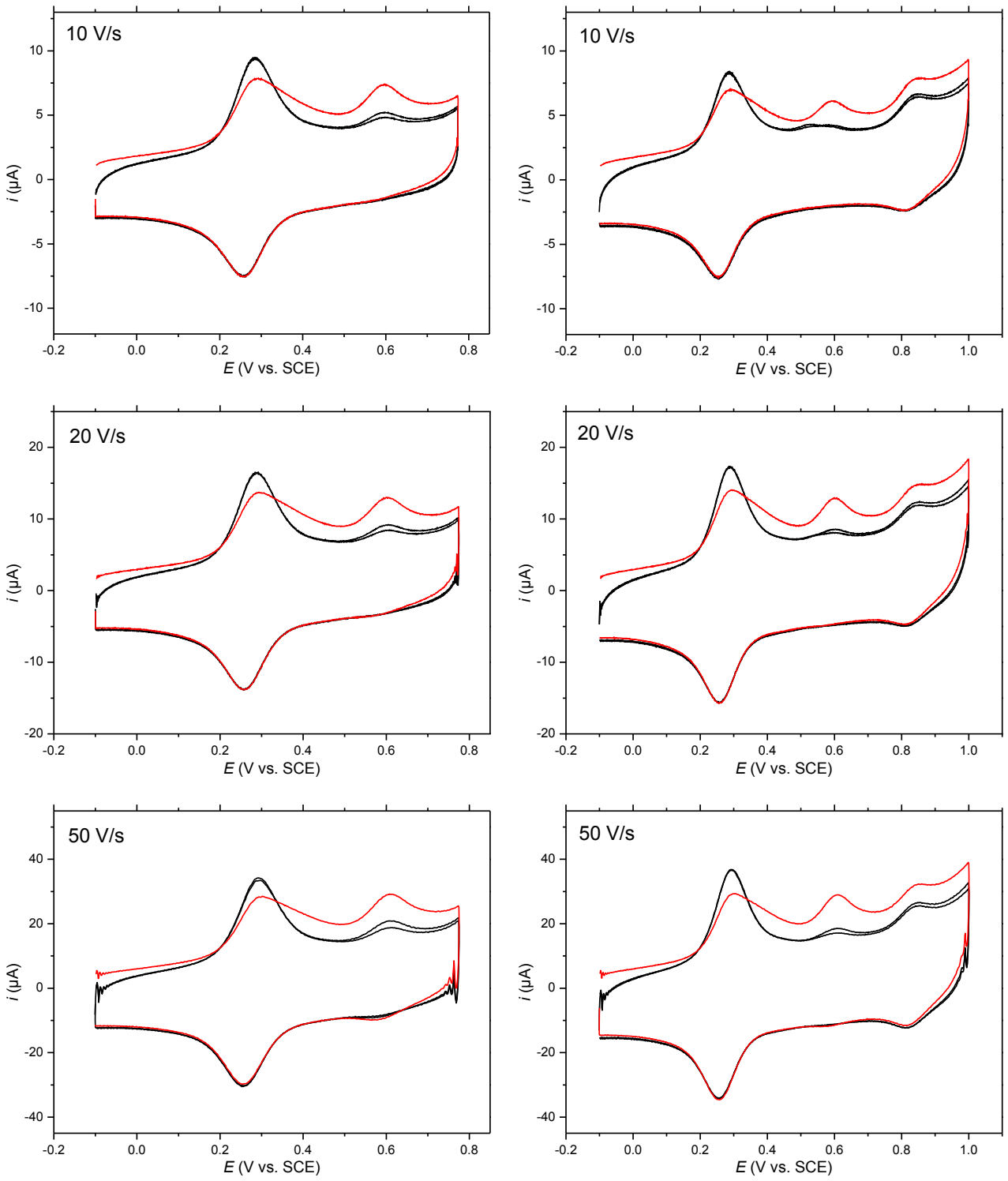

Figure S20. Cyclic voltammograms of complex **3** in aqueous TfOH at scan rates 10, 20, and 50 V/s. The first scan (red) and two consecutive (black) scans are shown. For details see Section 1.3.2.

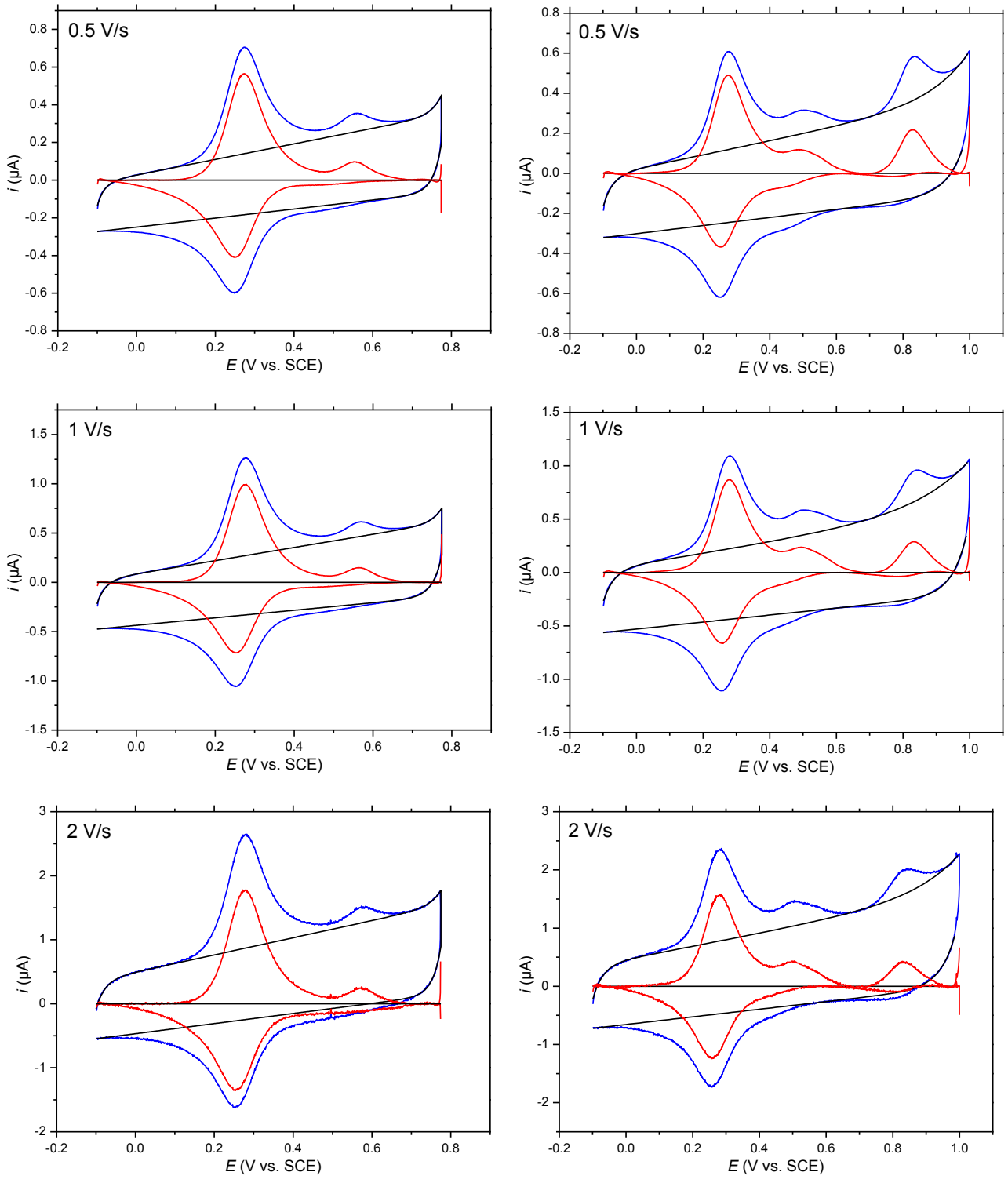

Figure S21. Cyclic voltammograms of complex **3** in aqueous TfOH at scan rates 0.5, 1, and 2 V/s. Experimental data (blue), simulated background current (black); and background-subtracted voltammograms (red) are shown. For details see Section 1.3.2.

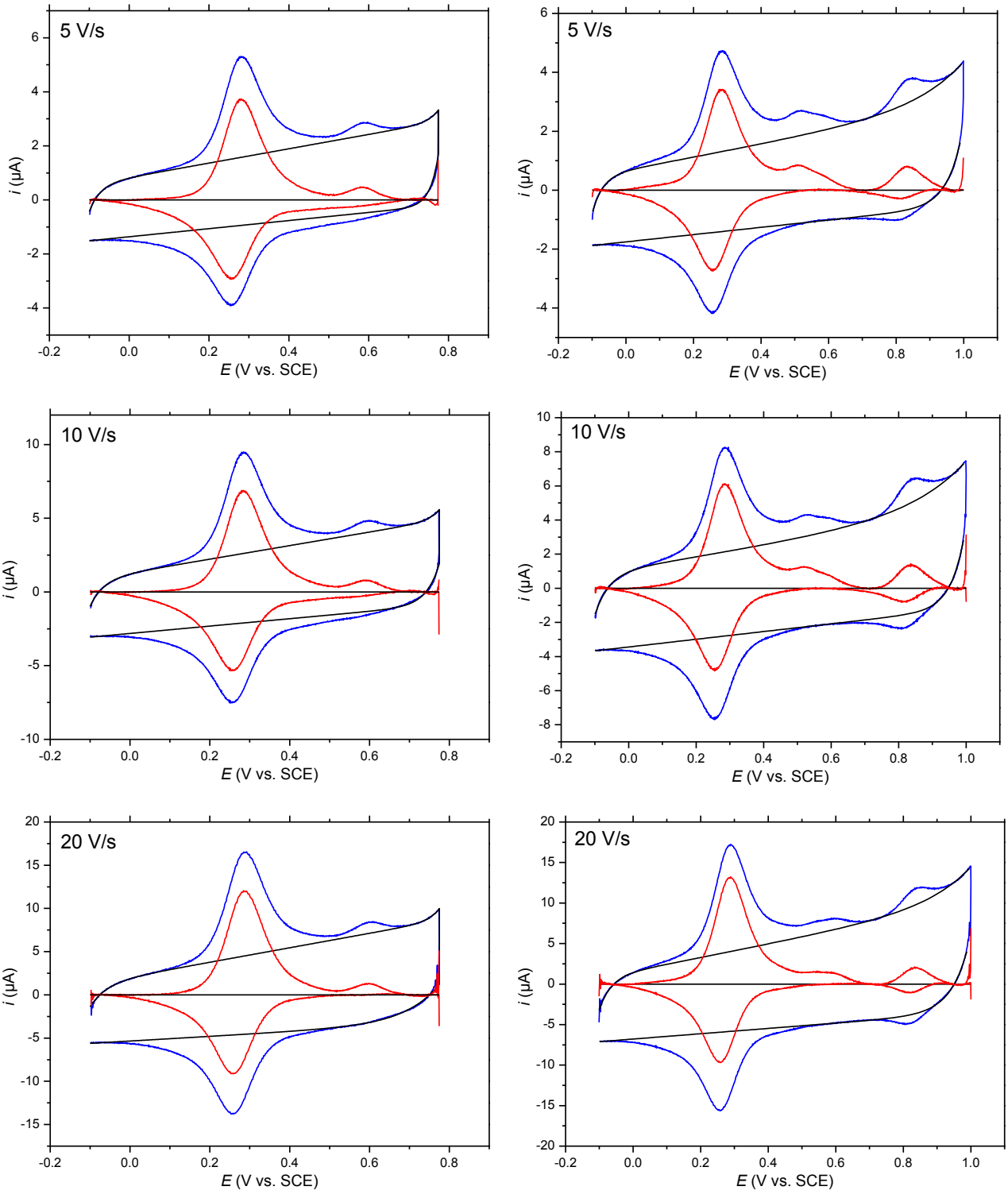

Figure S22. Cyclic voltammograms of complex **3** in aqueous TfOH at scan rates 5, 10, and 20 V/s. Experimental data (blue), simulated background current (black); and background-subtracted voltammograms (red) are shown. For details see Section 1.3.2.

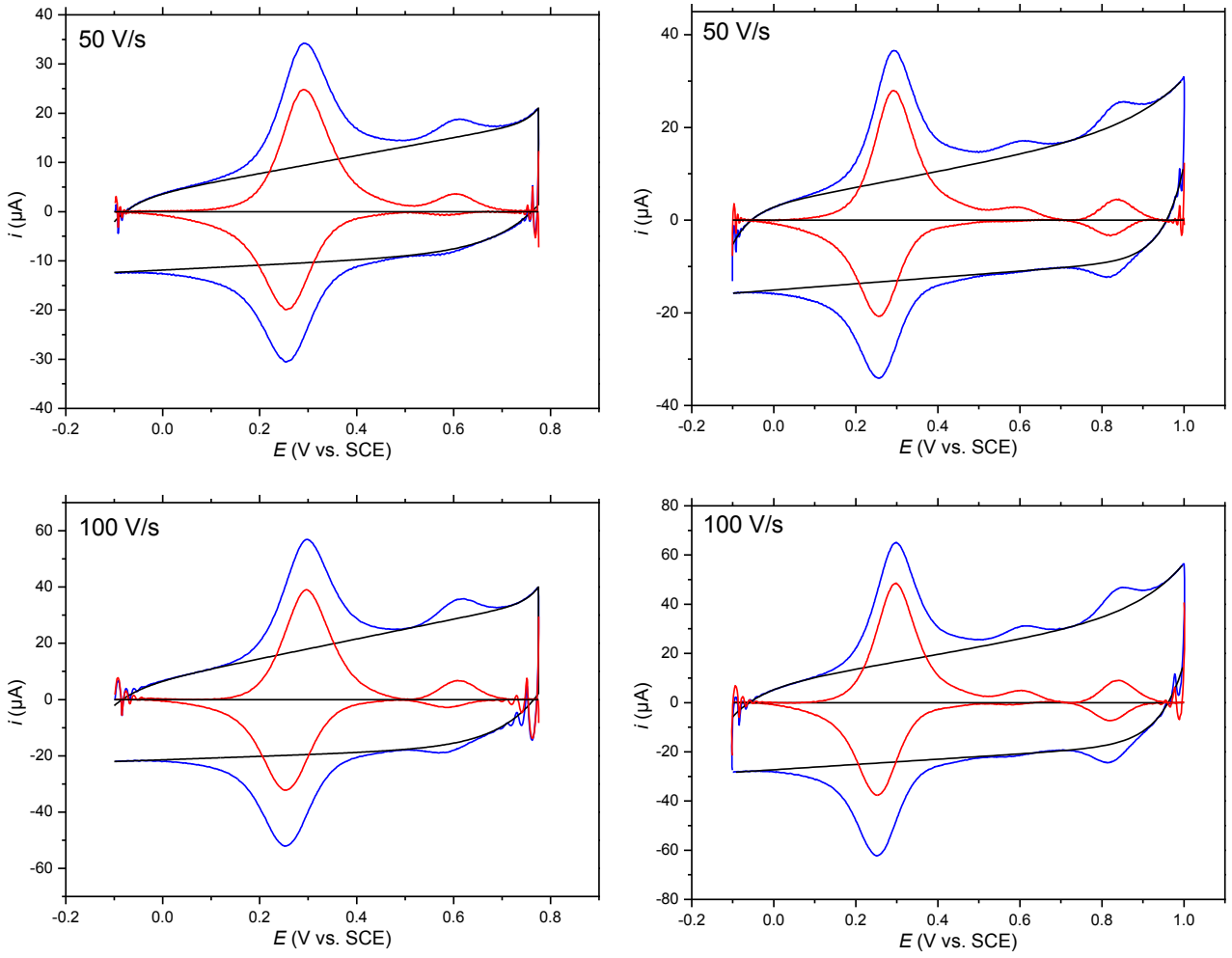

Figure S23. Cyclic voltammograms of complex **3** in aqueous TfOH at scan rates 50 and 100 V/s. Experimental data (blue), simulated background current (black); and background-subtracted voltammograms (red) are shown. For details see Section 1.3.2.

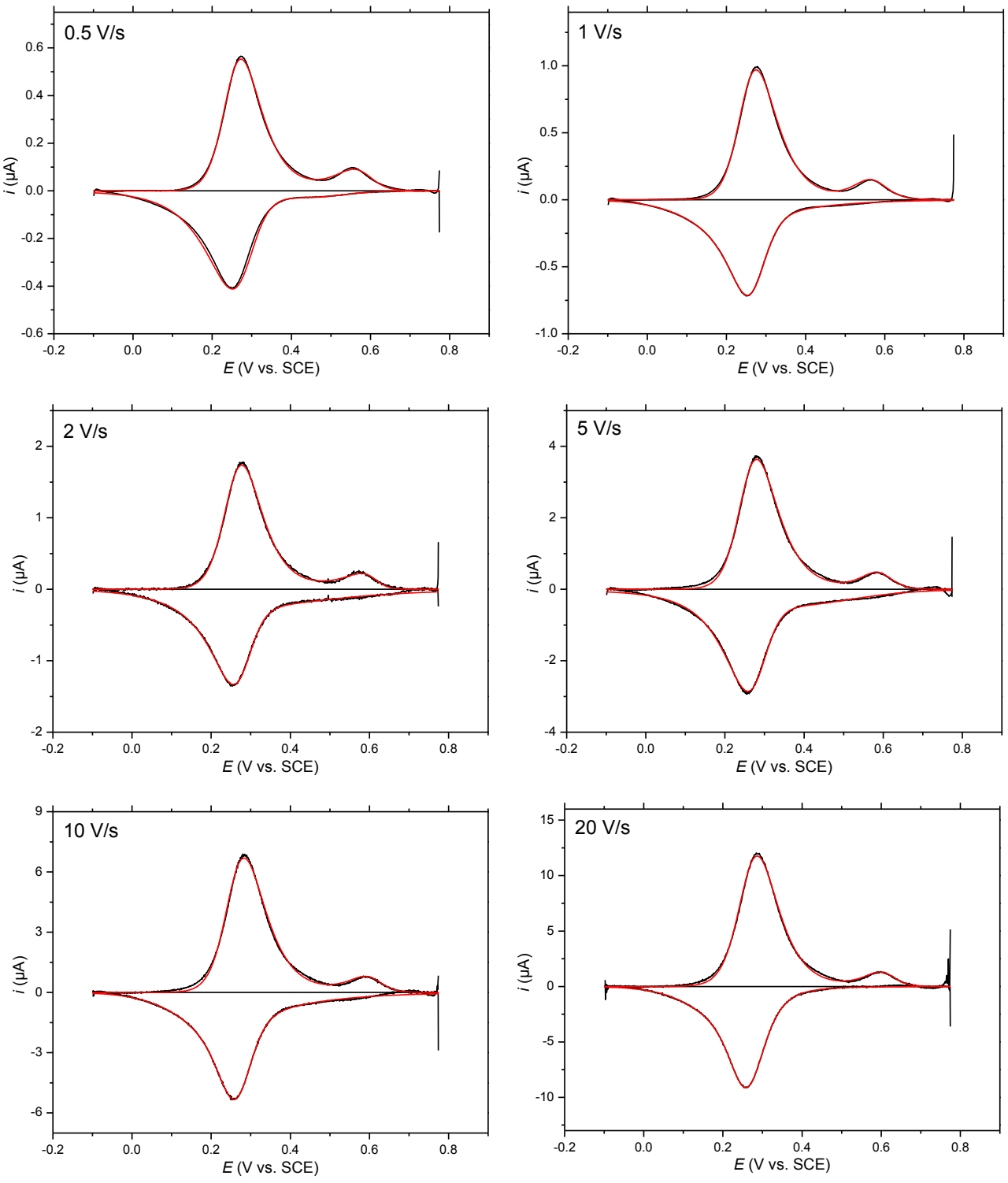

Figure S24. Cyclic voltammograms of complex **3** in aqueous TfOH at scan rates: 0.5, 1, 2, 5, 10, and 20 V/s. Experimental background-subtracted data (black) and simulated current (red) are shown. For details see Section 1.3.3.

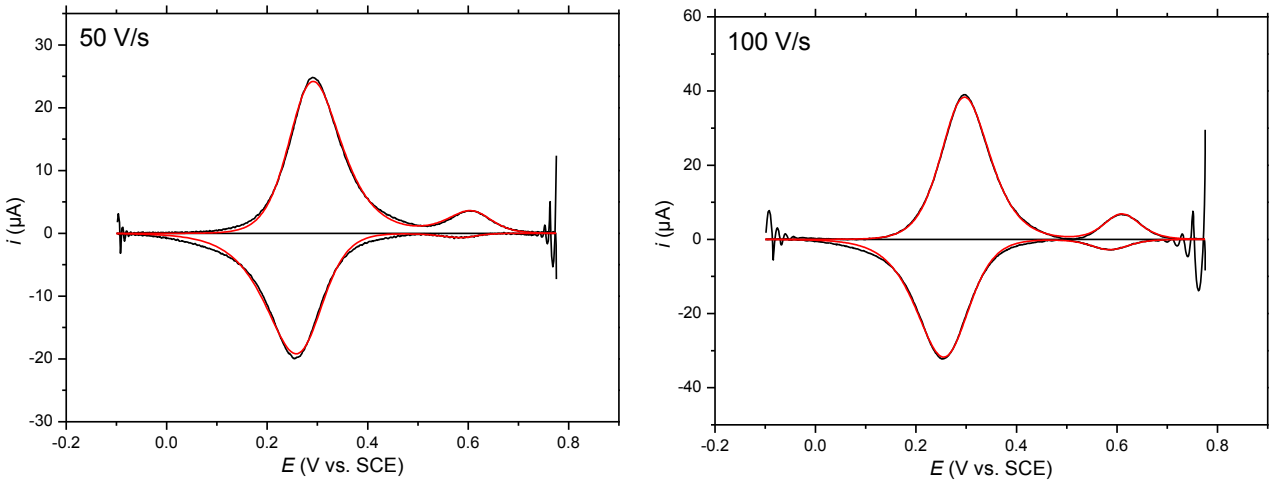

Figure S25. Cyclic voltammograms of complex **3** in aqueous TfOH at scan rates: 50 and 100 V/s. Experimental background-subtracted data (black) and simulated current (red) are shown. For details see Section 1.3.3.

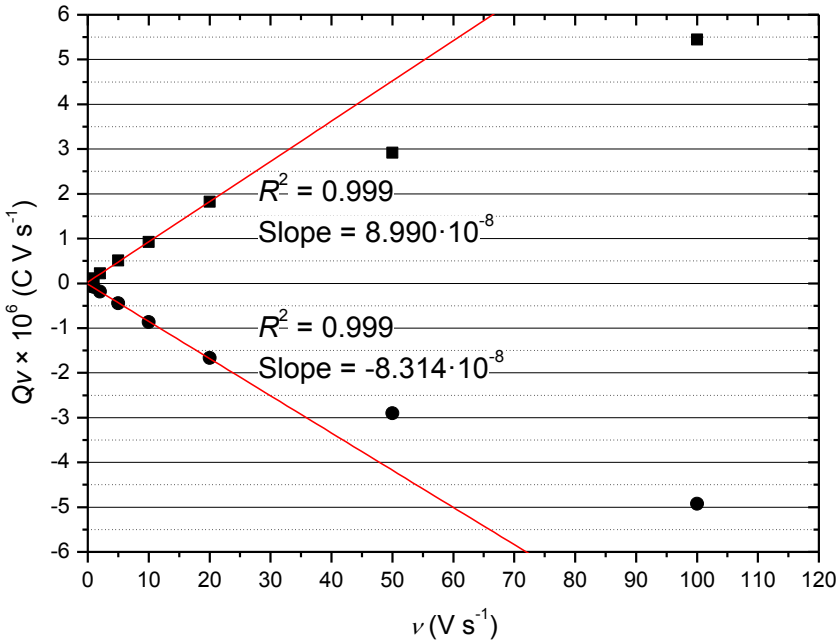

Figure S26. Dependence of the peak areas (Qv) on the scan rate (v) used for determination of the surface loading of **3**. For details see Section 1.3.3.

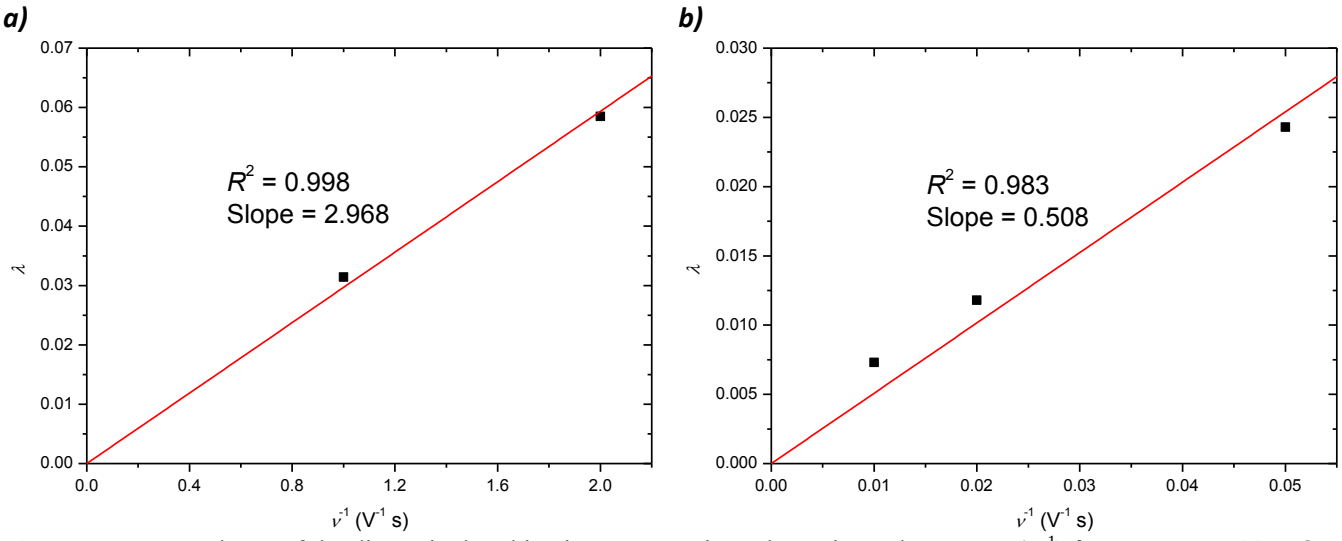

Figure S27. Dependence of the dimensionless kinetic parameter λ on the reciprocal scan rate (v^{-1}) for reactions 2 (a) and 3 (b). For details see Section 1.3.4.

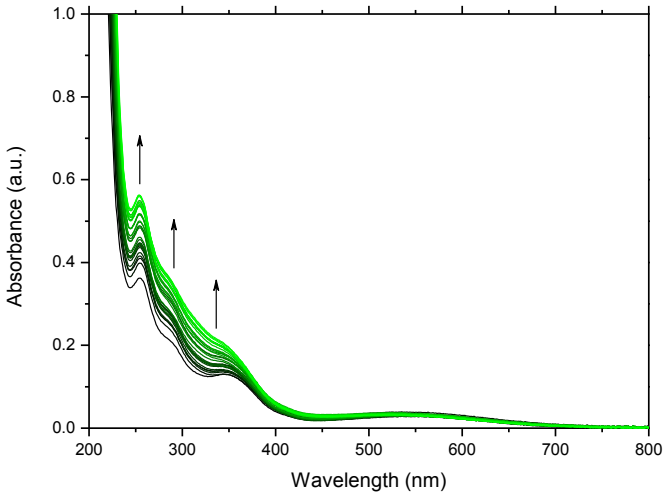

Figure S28. Spectrophotometric redox titration of complex **3** (0.1 mM, 1 mm quartz cuvette) with CAN. Arrows indicate direction of change in absorbance of complex **3** upon mixing with 2 to 8 equiv. of CAN.

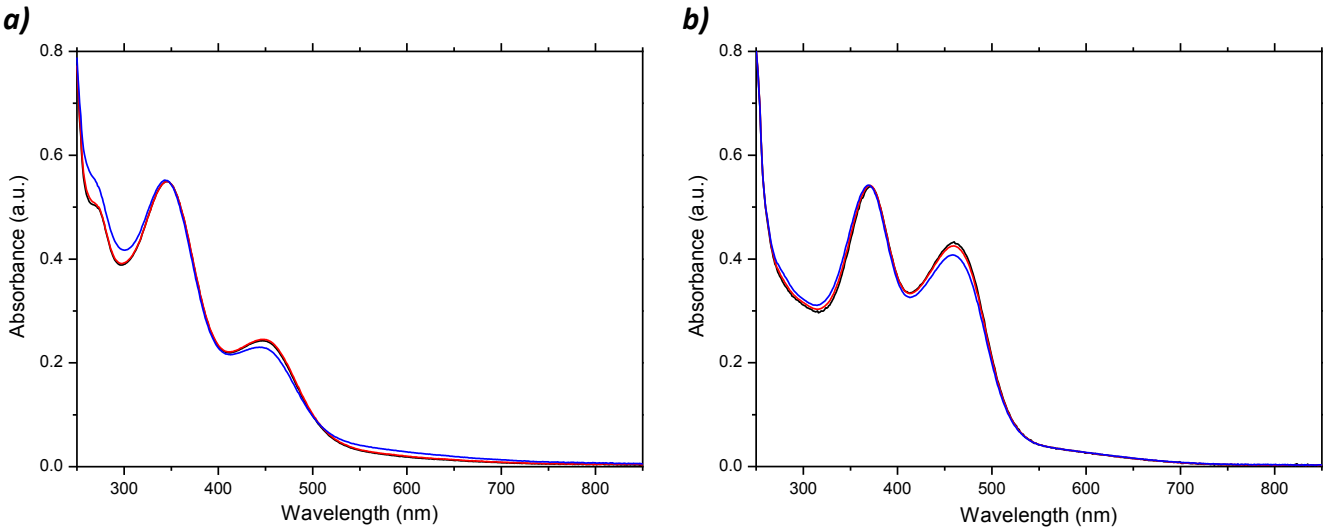

Figure S29. UV-vis absorption spectra of complex **3** (20 µM, 10 mm quartz cuvette) in (a) TfOH (0.1 M) containing 10% MeCN; (b) phosphate buffer (25 mM, pH 7.0) containing 10% MeCN. The measurements were carried out under inert conditions (black), after 3 min of purging with oxygen (red), and letting the solutions stand under an oxygen atmosphere for 60 min (blue).

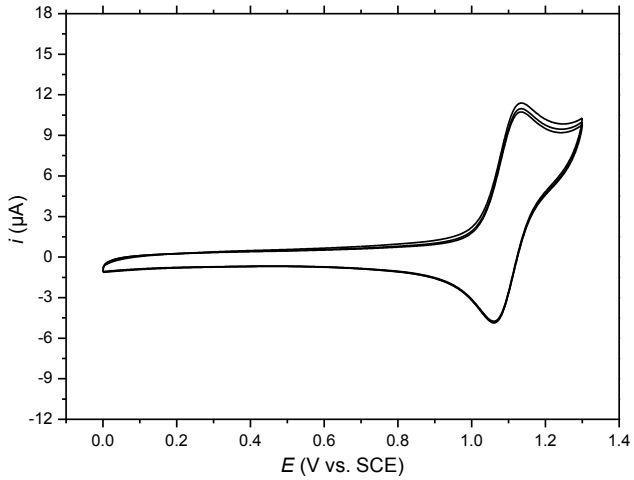

Figure S30. Cyclic voltammograms of ruthenium photosensitizer $[Ru(bpy)_2(bdc)](PF_6)_2$ (1 mM) in phosphate buffer (0.1 M, pH 7.0) containing 10% MeCN. Scan rate 0.05 V s^{-1}, glassy carbon (d = 3 mm) was used as working electrode, platinum coil as the counter electrode, and SCE as the reference electrode.

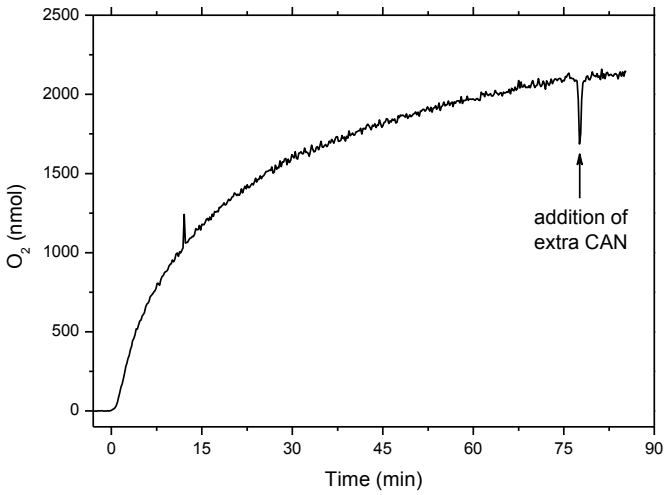

Figure S31. Oxygen evolution catalyzed by complex **3** using CAN as chemical oxidant. Conditions are as described in Figure 13.

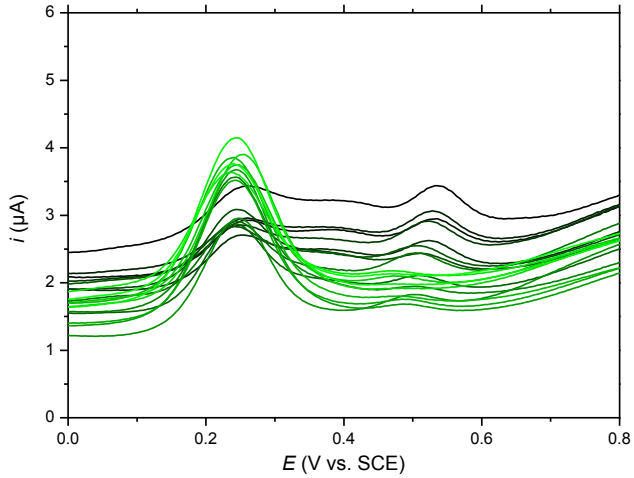

Figure S32. SWV of complex **3** at pH varying from 0.2 (black line) to 2.0 (green line). For details see Section 1.3.2.

4. Structure Determination of Complex 3 by Single Crystal X-ray Diffraction (SC-XRD)

Single crystals of complex **3** were obtained by slow evaporation of the MeCN solution. A suitable crystal was selected and mounted on a glass fiber with two-component glue on a Xcalibur III diffractometer with 4-circle kappa geometry. The crystal was kept at 298 K during data collection. Using Olex2[S12], the structure was solved with the ShelXT[S13] structure solution program using Direct Methods and refined with the olex2.refine[S14] refinement package using Gauss-Newton minimization.

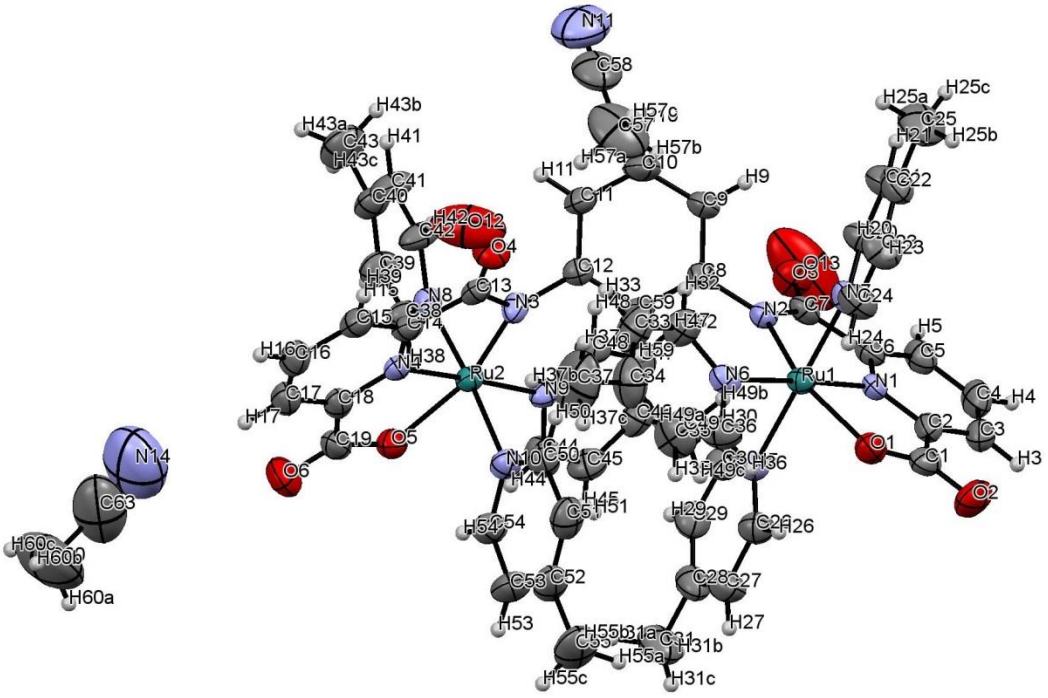

Figure S33. X-ray crystal structure of complex **3** (ellipsoids at 50% probability).

Table S2. Crystal data and structure refinement for single crystal of complex **3**.

Identification code	p21a_a
Empirical formula	$C_{60}H_{58}N_{12}O_8Ru_2$
Formula weight	1277.34
Temperature/K	298
Crystal system	monoclinic
Space group	$P2_1/c$
a/Å	10.7785(7)
b/Å	23.8622(11)
c/Å	23.4218(15)
β/°	100.611(6)
Volume/Å^3	5921.0(6)
Z	4
ρ_{calc}g/cm^3	1.4328
μ/mm^{-1}	0.574
F(000)	2607.1
Crystal size/mm^3	0.1 × 0.1 × 0.08
Radiation	Mo Kα (λ = 0.71073)
2Θ range for data collection/°	6.4 to 50.06

Index ranges	$-14 \leq h \leq 13$, $-31 \leq k \leq 31$, $-31 \leq l \leq 21$
Reflections collected	39673
Independent reflections	10441 [R_{int} = 0.0890, R_{sigma} = 0.0975]
Data/restraints/parameters	10441/0/747
Goodness-of-fit on F^2	1.013
Final R indexes [$I>=2\sigma$ (I)]	R_1 = 0.0628, wR_2 = 0.1524
Final R indexes [all data]	R_1 = 0.0884, wR_2 = 0.1740
Largest diff. peak/hole / e Å^{-3}	1.41/-0.95

Table S3. Fractional atomic coordinates ($\times 10^4$) and equivalent isotropic displacement parameters (Å$^2\times 10^3$) for single crystal of complex **3**. U_{eq} is defined as 1/3 of of the trace of the orthogonalised U_{IJ} tensor.

Atom	***x***	***y***	***z***	**U(eq)**
Ru1	2117.0(4)	5114.96(17)	7208.29(19)	31.00(16)
Ru2	4054.6(4)	7605.04(17)	6171.94(19)	30.22(16)
O1	474(4)	4594.2(16)	7112.7(18)	43.9(10)
O2	-137(5)	3724.5(19)	6819(2)	66.3(14)
O3	5812(4)	4969.8(17)	6927(2)	52.7(11)
O4	3692(4)	7729.1(17)	7920.6(17)	47.9(10)
O5	3769(4)	8138.8(16)	5427.5(17)	41.6(9)
O6	3190(5)	9019.3(19)	5180(2)	67.7(14)
N1	2762(4)	4428.4(17)	6915.9(18)	31.1(10)
N2	4009(4)	5337.2(17)	7201.5(19)	31.9(10)
N3	4146(4)	7368.8(17)	7052.1(19)	34.9(11)
N4	3472(4)	8284.1(16)	6501.3(19)	30.5(10)
N5	1568(4)	5387.1(18)	6338(2)	36.3(10)
N6	1280(4)	5833.3(18)	7524(2)	36.3(11)
N7	2586(5)	4859.7(18)	8083(2)	39.4(11)
N8	5915(4)	7892.5(17)	6326.3(19)	34.1(10)
N9	4696(4)	6889.5(17)	5768.7(19)	32.4(10)
N10	2165(4)	7348.8(18)	5934(2)	39.6(11)
C1	653(6)	4102(3)	6912(3)	44.4(15)
C2	1967(6)	3993(2)	6785(2)	42.0(14)
C3	2390(7)	3506(2)	6551(3)	50.8(16)
C4	3625(7)	3471(2)	6478(3)	53.2(17)
C5	4433(6)	3922(2)	6623(3)	46.5(15)
C6	3957(5)	4401(2)	6838(2)	36.5(13)
C7	4701(5)	4936(2)	7001(2)	37.3(13)
C8	4630(5)	5852(2)	7381(2)	30.1(11)
C9	5713(5)	5862(2)	7811(2)	40.9(14)

C10	6251(6)	6376(3)	7995(3)	50.9(16)
C11	5724(5)	6872(2)	7771(3)	40.5(14)
C12	4662(5)	6868(2)	7330(2)	30.7(12)
C13	3748(5)	7766(2)	7394(2)	33.7(12)
C14	3336(5)	8298(2)	7060(2)	35.9(13)
C15	2869(5)	8777(2)	7288(3)	44.2(15)
C16	2566(6)	9241(2)	6926(3)	52.0(17)
C17	2722(6)	9216(2)	6351(3)	48.0(16)
C18	3173(5)	8727(2)	6143(3)	39.7(14)
C19	3389(6)	8637(3)	5534(3)	45.2(15)
C20	3727(6)	4724(3)	8351(3)	45.8(15)
C21	4052(7)	4604(3)	8933(3)	55.5(17)
C22	3146(7)	4616(3)	9276(3)	58.7(18)
C23	1934(7)	4748(3)	8998(3)	60.1(18)
C24	1688(6)	4864(3)	8416(3)	50.2(16)
C25	3444(9)	4505(4)	9927(3)	85(3)
C26	356(6)	5379(3)	6087(3)	47.7(15)
C27	-62(7)	5551(3)	5512(3)	62.2(19)
C28	770(8)	5735(3)	5179(3)	58.4(18)
C29	2015(7)	5729(3)	5442(3)	52.7(16)
C30	2384(6)	5553(2)	6003(3)	44.3(14)
C31	327(9)	5928(4)	4570(3)	87(3)
C32	1902(6)	6218(3)	7874(3)	50.4(16)
C33	1337(8)	6669(3)	8074(4)	71(2)
C34	60(8)	6743(3)	7932(4)	69(2)
C35	-614(7)	6337(3)	7577(4)	70(2)
C36	25(6)	5900(3)	7389(3)	57.2(18)
C37	-584(9)	7244(4)	8160(5)	117(4)
C38	6497(6)	7969(3)	5871(3)	50.0(16)
C39	7724(6)	8146(3)	5931(3)	56.0(17)
C40	8420(6)	8264(3)	6460(3)	50.2(16)
C41	7814(6)	8204(3)	6927(3)	57.7(18)
C42	6594(6)	8018(3)	6848(3)	52.0(16)
C43	9776(7)	8460(3)	6558(4)	81(3)
C44	4369(6)	6817(3)	5187(3)	48.7(15)
C45	4785(6)	6381(3)	4887(3)	51.9(16)
C46	5576(6)	5983(2)	5175(3)	48.3(16)
C47	5890(6)	6043(2)	5774(3)	48.7(16)
C48	5468(5)	6497(2)	6043(3)	40.3(14)
C49	6100(7)	5515(3)	4841(3)	64(2)

C50	1477(6)	7125(2)	6294(3)	45.7(15)
C51	234(6)	6960(3)	6122(3)	57.8(18)
C52	-375(6)	7031(3)	5553(4)	60.3(19)
C53	316(7)	7266(3)	5186(4)	64(2)
C54	1552(6)	7418(3)	5383(3)	51.9(16)
C55	-1719(7)	6842(4)	5339(4)	90(3)
C59	4119(5)	6353(2)	7148(2)	29.8(11)
N11	7036(11)	7076(5)	9384(4)	119(3)
C57	4706(12)	6823(5)	9097(4)	117(4)
C58	6043(12)	6970(4)	9264(4)	85(3)
C60	-230(14)	11147(7)	5404(7)	195(7)
O12	2408(6)	8117(4)	8760(3)	125(3)
O13	7577(9)	4700(4)	6302(4)	181(5)
N14	1198(14)	10489(6)	6090(8)	199(7)
C63	523(13)	10761(6)	5770(9)	151(6)

Table S4. Anisotropic displacement parameters ($Å^2 \times 10^3$) for single crystal of complex **3**. The anisotropic displacement factor exponent takes the form: $-2\pi^2[h^2a^{*2}U_{11}+2hka^*b^*U_{12}+\ldots]$.

Atom	U_{11}	U_{22}	U_{33}	U_{12}	U_{13}	U_{23}
Ru1	26.0(3)	32.4(3)	33.8(3)	2.69(17)	3.17(19)	1.84(18)
Ru2	27.3(3)	31.7(3)	30.8(3)	-3.26(17)	2.92(18)	-1.88(17)
O1	33(2)	45(2)	52(3)	-4.5(17)	4.8(19)	8.4(19)
O2	59(3)	65(3)	71(3)	-32(2)	4(3)	2(2)
O3	32(2)	60(3)	69(3)	6.2(19)	17(2)	-5(2)
O4	59(3)	54(2)	33(2)	8(2)	13(2)	-3.4(18)
O5	43(2)	43(2)	37(2)	-6.0(18)	2.4(18)	2.5(17)
O6	88(4)	54(3)	58(3)	4(2)	4(3)	19(2)
N1	32(3)	29(2)	30(2)	0.6(18)	0.0(19)	6.7(18)
N2	29(2)	31(2)	34(3)	1.9(19)	3(2)	1.3(19)
N3	47(3)	29(2)	30(3)	-6(2)	10(2)	-2.9(19)
N4	24(2)	31(2)	35(3)	-5.7(17)	1.9(19)	-0.0(19)
N5	34(3)	37(2)	36(3)	0(2)	1(2)	0(2)
N6	30(3)	41(3)	39(3)	4(2)	9(2)	5(2)
N7	41(3)	37(3)	41(3)	6(2)	9(2)	6(2)
N8	33(3)	33(2)	36(3)	-2.1(19)	3(2)	-2.0(19)
N9	32(3)	37(2)	29(3)	-6.4(19)	7(2)	-2.5(19)
N10	28(3)	38(3)	52(3)	-0.6(19)	4(2)	-4(2)
C1	47(4)	50(4)	33(3)	-9(3)	-2(3)	12(3)
C2	56(4)	32(3)	34(3)	-3(3)	-1(3)	3(2)

C3	67(5)	36(3)	45(4)	-7(3)	-2(3)	4(3)
C4	74(5)	34(3)	51(4)	10(3)	9(4)	-8(3)
C5	54(4)	40(3)	45(4)	14(3)	8(3)	-1(3)
C6	39(3)	39(3)	30(3)	10(2)	0(2)	6(2)
C7	31(3)	39(3)	40(3)	11(2)	3(3)	7(2)
C8	26(3)	33(3)	32(3)	3(2)	7(2)	2(2)
C9	37(3)	42(3)	38(3)	4(3)	-5(3)	5(3)
C10	37(4)	59(4)	49(4)	1(3)	-13(3)	-3(3)
C11	35(3)	43(3)	40(3)	-3(2)	-1(3)	-10(3)
C12	26(3)	36(3)	32(3)	0(2)	8(2)	-2(2)
C13	24(3)	37(3)	38(3)	-6(2)	3(2)	-7(2)
C14	27(3)	39(3)	40(3)	-2(2)	-1(2)	-7(2)
C15	35(3)	43(3)	52(4)	-1(3)	1(3)	-13(3)
C16	46(4)	35(3)	72(5)	4(3)	2(3)	-8(3)
C17	42(4)	36(3)	62(4)	0(3)	1(3)	5(3)
C18	27(3)	34(3)	56(4)	-3(2)	2(3)	4(3)
C19	37(4)	44(4)	50(4)	-5(3)	-2(3)	13(3)
C20	41(4)	55(4)	40(4)	15(3)	6(3)	5(3)
C21	52(4)	71(4)	41(4)	12(3)	4(3)	6(3)
C22	81(5)	47(4)	45(4)	9(3)	5(4)	6(3)
C23	62(5)	70(4)	54(5)	6(4)	26(4)	10(3)
C24	39(4)	63(4)	51(4)	10(3)	15(3)	11(3)
C25	116(8)	95(6)	42(5)	4(5)	10(5)	12(4)
C26	40(4)	52(4)	50(4)	2(3)	4(3)	1(3)
C27	61(5)	62(4)	56(5)	10(3)	-12(4)	3(3)
C28	87(6)	49(4)	35(4)	6(4)	2(4)	1(3)
C29	66(5)	54(4)	41(4)	-2(3)	16(3)	2(3)
C30	48(4)	49(3)	37(4)	-3(3)	10(3)	2(3)
C31	125(8)	82(6)	45(5)	13(5)	-8(5)	6(4)
C32	34(3)	54(4)	67(5)	-1(3)	19(3)	-10(3)
C33	71(6)	55(4)	94(6)	-10(4)	32(5)	-29(4)
C34	74(6)	46(4)	97(6)	14(4)	40(5)	-1(4)
C35	51(5)	67(5)	94(6)	26(4)	17(4)	-10(4)
C36	47(4)	68(4)	54(4)	13(3)	3(3)	-5(3)
C37	95(8)	74(6)	194(13)	28(5)	54(8)	-31(7)
C38	38(4)	65(4)	46(4)	-5(3)	8(3)	3(3)
C39	41(4)	68(4)	60(5)	-11(3)	13(3)	0(3)
C40	31(3)	49(4)	68(5)	-6(3)	3(3)	-12(3)
C41	46(4)	76(5)	47(4)	-19(3)	-1(3)	-17(3)
C42	50(4)	71(4)	33(4)	-21(3)	3(3)	-13(3)

C43	41(4)	81(5)	119(8)	-11(4)	11(5)	-15(5)
C44	54(4)	52(4)	38(4)	6(3)	6(3)	-3(3)
C45	52(4)	62(4)	41(4)	-2(3)	8(3)	-16(3)
C46	46(4)	43(3)	60(4)	-7(3)	21(3)	-11(3)
C47	50(4)	44(3)	56(4)	6(3)	20(3)	9(3)
C48	37(3)	52(3)	32(3)	1(3)	7(3)	0(3)
C49	69(5)	63(4)	66(5)	2(4)	29(4)	-20(4)
C50	37(3)	45(3)	55(4)	-1(3)	7(3)	5(3)
C51	46(4)	48(4)	83(6)	-7(3)	21(4)	5(3)
C52	36(4)	49(4)	91(6)	-6(3)	-2(4)	3(4)
C53	48(4)	65(4)	70(5)	-13(3)	-12(4)	-3(4)
C54	41(4)	56(4)	54(4)	-10(3)	-1(3)	5(3)
C55	39(4)	79(6)	146(9)	-16(4)	-3(5)	2(5)
C59	21(3)	37(3)	29(3)	0(2)	-2(2)	-1(2)
N11	133(9)	142(8)	71(6)	-17(7)	-7(6)	-19(5)
C57	150(11)	152(10)	58(6)	35(8)	42(7)	18(6)
C58	114(9)	100(7)	38(5)	3(6)	3(6)	0(4)
C60	146(14)	201(16)	211(18)	46(12)	-33(12)	70(14)
O12	95(5)	210(8)	69(4)	53(5)	11(4)	-34(5)
O13	148(8)	237(10)	196(9)	95(7)	132(7)	109(8)
N14	157(13)	162(12)	273(19)	46(9)	29(12)	30(12)
C63	87(9)	123(11)	250(20)	10(8)	45(11)	38(11)

Table S5. Bond lengths for single crystal of complex **3**.

Atom	**Atom**	**Length/Å**	**Atom**	**Atom**	**Length/Å**
Ru1	O1	2.141(4)	C8	C59	1.387(7)
Ru1	N1	1.952(4)	C9	C10	1.389(8)
Ru1	N2	2.110(4)	C10	C11	1.375(8)
Ru1	N5	2.118(5)	C11	C12	1.394(7)
Ru1	N6	2.132(4)	C12	C59	1.392(7)
Ru1	N7	2.108(5)	C13	C14	1.513(8)
Ru2	O5	2.135(4)	C14	C15	1.395(8)
Ru2	N3	2.122(4)	C15	C16	1.396(9)
Ru2	N4	1.948(4)	C16	C17	1.389(9)
Ru2	N8	2.087(4)	C17	C18	1.385(8)
Ru2	N9	2.127(4)	C18	C19	1.503(9)
Ru2	N10	2.101(5)	C20	C21	1.373(8)
O1	C1	1.292(7)	C21	C22	1.376(9)
O2	C1	1.232(7)	C22	C23	1.384(10)

O3	C7	1.244(7)	C22	C25	1.521(9)
O4	C13	1.250(7)	C23	C24	1.369(9)
O5	C19	1.296(7)	C26	C27	1.401(9)
O6	C19	1.225(7)	C27	C28	1.366(10)
N1	C2	1.346(7)	C28	C29	1.370(10)
N1	C6	1.336(7)	C28	C31	1.491(9)
N2	C7	1.350(7)	C29	C30	1.366(8)
N2	C8	1.425(7)	C32	C33	1.362(9)
N3	C12	1.425(7)	C33	C34	1.367(11)
N3	C13	1.360(7)	C34	C35	1.391(11)
N4	C14	1.345(7)	C34	C37	1.528(10)
N4	C18	1.351(7)	C35	C36	1.366(9)
N5	C26	1.329(7)	C38	C39	1.371(8)
N5	C30	1.341(7)	C39	C40	1.354(9)
N6	C32	1.327(8)	C40	C41	1.381(9)
N6	C36	1.340(8)	C40	C43	1.511(9)
N7	C20	1.315(7)	C41	C42	1.367(9)
N7	C24	1.349(7)	C44	C45	1.376(8)
N8	C38	1.345(7)	C45	C46	1.368(9)
N8	C42	1.337(7)	C46	C47	1.389(9)
N9	C44	1.353(7)	C46	C49	1.530(8)
N9	C48	1.337(7)	C47	C48	1.372(8)
N10	C50	1.333(7)	C50	C51	1.383(9)
N10	C54	1.347(8)	C51	C52	1.382(10)
C1	C2	1.522(9)	C52	C53	1.357(10)
C2	C3	1.397(8)	C52	C55	1.513(9)
C3	C4	1.375(9)	C53	C54	1.376(9)
C4	C5	1.385(9)	N11	C58	1.085(13)
C5	C6	1.387(8)	C57	C58	1.465(15)
C6	C7	1.518(8)	C60	C63	1.410(18)
C8	C9	1.393(7)	N14	C63	1.145(17)

Table S6. Bond angles for single crystal of complex **3**.

Atom	**Atom**	**Atom**	**Angle/°**	**Atom**	**Atom**	**Atom**	**Angle/°**
N1	Ru1	O1	79.48(16)	C7	C6	C5	124.9(5)
N2	Ru1	O1	157.98(16)	N2	C7	O3	127.6(5)
N2	Ru1	N1	78.53(17)	C6	C7	O3	119.8(5)
N5	Ru1	O1	89.89(16)	C6	C7	N2	112.5(5)
N5	Ru1	N1	88.51(17)	C9	C8	N2	121.0(5)

N5	Ru1	N2	90.85(17)	C59	C8	N2	119.8(5)
N6	Ru1	O1	96.21(16)	C59	C8	C9	119.2(5)
N6	Ru1	N1	175.70(17)	C10	C9	C8	119.1(5)
N6	Ru1	N2	105.77(17)	C11	C10	C9	121.5(6)
N6	Ru1	N5	91.49(17)	C12	C11	C10	120.0(5)
N7	Ru1	O1	88.82(17)	C11	C12	N3	122.0(5)
N7	Ru1	N1	93.51(17)	C59	C12	N3	119.6(5)
N7	Ru1	N2	91.20(17)	C59	C12	C11	118.4(5)
N7	Ru1	N5	177.36(17)	N3	C13	O4	127.6(5)
N7	Ru1	N6	86.36(17)	C14	C13	O4	120.4(5)
N3	Ru2	O5	157.78(16)	C14	C13	N3	112.1(5)
N4	Ru2	O5	79.56(17)	C13	C14	N4	114.1(5)
N4	Ru2	N3	78.29(17)	C15	C14	N4	120.3(5)
N8	Ru2	O5	86.27(16)	C15	C14	C13	125.7(5)
N8	Ru2	N3	92.73(17)	C16	C15	C14	118.6(6)
N8	Ru2	N4	91.59(16)	C17	C16	C15	119.8(6)
N9	Ru2	O5	97.23(16)	C18	C17	C16	119.5(6)
N9	Ru2	N3	104.91(16)	C17	C18	N4	119.9(6)
N9	Ru2	N4	176.76(17)	C19	C18	N4	114.6(5)
N9	Ru2	N8	87.73(16)	C19	C18	C17	125.5(5)
N10	Ru2	O5	88.28(17)	O6	C19	O5	125.1(6)
N10	Ru2	N3	92.87(19)	C18	C19	O5	115.1(5)
N10	Ru2	N4	88.84(17)	C18	C19	O6	119.8(6)
N10	Ru2	N8	174.35(18)	C21	C20	N7	124.7(6)
N10	Ru2	N9	91.53(17)	C22	C21	C20	119.9(6)
C1	O1	Ru1	112.9(4)	C23	C22	C21	116.0(6)
C19	O5	Ru2	113.1(4)	C25	C22	C21	122.7(7)
C2	N1	Ru1	118.3(4)	C25	C22	C23	121.2(7)
C6	N1	Ru1	120.2(4)	C24	C23	C22	120.5(6)
C6	N1	C2	121.4(5)	C23	C24	N7	123.1(6)
C7	N2	Ru1	114.9(4)	C27	C26	N5	122.4(6)
C8	N2	Ru1	128.1(3)	C28	C27	C26	121.0(7)
C8	N2	C7	117.0(4)	C29	C28	C27	115.5(6)
C12	N3	Ru2	127.7(3)	C31	C28	C27	121.2(8)
C13	N3	Ru2	115.0(4)	C31	C28	C29	123.3(7)
C13	N3	C12	117.1(4)	C30	C29	C28	121.6(6)
C14	N4	Ru2	120.5(3)	C29	C30	N5	123.2(6)
C18	N4	Ru2	117.5(4)	C33	C32	N6	123.5(6)
C18	N4	C14	121.9(5)	C34	C33	C32	120.8(7)
C26	N5	Ru1	119.9(4)	C35	C34	C33	116.6(6)

C30	N5	Ru1	123.8(4)	C37	C34	C33	121.1(8)
C30	N5	C26	116.3(5)	C37	C34	C35	122.3(8)
C32	N6	Ru1	124.9(4)	C36	C35	C34	119.0(7)
C36	N6	Ru1	119.1(4)	C35	C36	N6	124.2(7)
C36	N6	C32	115.8(5)	C39	C38	N8	122.8(6)
C20	N7	Ru1	124.8(4)	C40	C39	C38	121.3(7)
C24	N7	Ru1	119.3(4)	C41	C40	C39	116.1(6)
C24	N7	C20	115.7(5)	C43	C40	C39	124.1(7)
C38	N8	Ru2	118.7(4)	C43	C40	C41	119.8(7)
C42	N8	Ru2	125.4(4)	C42	C41	C40	120.6(6)
C42	N8	C38	115.9(5)	C41	C42	N8	123.2(6)
C44	N9	Ru2	120.2(4)	C45	C44	N9	124.2(6)
C48	N9	Ru2	125.0(4)	C46	C45	C44	120.3(6)
C48	N9	C44	114.7(5)	C47	C46	C45	116.2(6)
C50	N10	Ru2	125.0(4)	C49	C46	C45	120.7(6)
C54	N10	Ru2	119.9(4)	C49	C46	C47	123.1(6)
C54	N10	C50	115.0(5)	C48	C47	C46	120.3(6)
O2	C1	O1	125.7(6)	C47	C48	N9	124.3(6)
C2	C1	O1	115.7(5)	C51	C50	N10	123.5(6)
C2	C1	O2	118.6(6)	C52	C51	C50	120.5(6)
C1	C2	N1	113.5(5)	C53	C52	C51	116.3(6)
C3	C2	N1	119.4(6)	C55	C52	C51	122.6(7)
C3	C2	C1	127.0(5)	C55	C52	C53	121.1(8)
C4	C3	C2	119.5(6)	C54	C53	C52	120.5(7)
C5	C4	C3	120.1(6)	C53	C54	N10	124.2(7)
C6	C5	C4	118.2(6)	C12	C59	C8	121.8(5)
C5	C6	N1	121.3(5)	C57	C58	N11	179.3(12)
C7	C6	N1	113.8(5)	N14	C63	C60	174(2)

Table S7. Hydrogen atom coordinates ($Å \times 10^4$) and isotropic displacement parameters ($Å^2 \times 10^3$) for single crystal of complex **3**.

Atom	***x***	***y***	***z***	**U(eq)**
H3	1841(7)	3208(2)	6445(3)	61(2)
H4	3919(7)	3144(2)	6332(3)	64(2)
H5	5270(6)	3903(2)	6576(3)	55.7(18)
H9	6070(5)	5530(2)	7972(2)	49.0(17)
H10	6983(6)	6383(3)	8275(3)	61.0(19)
H11	6077(5)	7211(2)	7914(3)	48.5(16)
H15	2762(5)	8788(2)	7673(3)	53.0(18)

H16	2261(6)	9567(2)	7070(3)	62(2)
H17	2526(6)	9524(2)	6108(3)	57.5(19)
H20	4361(6)	4707(3)	8130(3)	55.0(18)
H21	4883(7)	4516(3)	9094(3)	67(2)
H23	1282(7)	4758(3)	9208(3)	72(2)
H24	864(6)	4950(3)	8241(3)	60.2(19)
H25a	3550(60)	4855(4)	10132(3)	127(4)
H25b	2760(30)	4300(20)	10039(6)	127(4)
H25c	4210(30)	4290(20)	10019(5)	127(4)
H26	-235(6)	5254(3)	6301(3)	57.2(18)
H27	-920(7)	5541(3)	5355(3)	75(2)
H29	2624(7)	5847(3)	5234(3)	63(2)
H30	3241(6)	5547(2)	6160(3)	53.2(17)
H31a	500(60)	6321(7)	4543(7)	131(4)
H31b	760(40)	5724(19)	4314(5)	131(4)
H31c	-564(14)	5860(20)	4461(10)	131(4)
H32	2770(6)	6177(3)	7989(3)	60.5(19)
H33	1826(8)	6931(3)	8310(4)	86(3)
H35	-1487(7)	6362(3)	7470(4)	84(3)
H36	-440(6)	5632(3)	7153(3)	69(2)
H37a	-390(70)	7250(20)	8577(5)	176(6)
H37b	-280(60)	7584(4)	8020(30)	176(6)
H37c	-1481(12)	7220(20)	8030(30)	176(6)
H38	6047(6)	7898(3)	5499(3)	60.0(19)
H39	8086(6)	8186(3)	5602(3)	67(2)
H41	8240(6)	8290(3)	7299(3)	69(2)
H42	6218(6)	7978(3)	7172(3)	62(2)
H43a	9833(11)	8829(11)	6720(20)	121(4)
H43b	10291(11)	8207(15)	6820(20)	121(4)
H43c	10066(19)	8470(20)	6195(5)	121(4)
H44	3830(6)	7079(3)	4977(3)	58.4(19)
H45	4527(6)	6357(3)	4486(3)	62(2)
H47	6388(6)	5773(2)	5994(3)	58.4(19)
H48	5737(5)	6534(2)	6442(3)	48.3(16)
H49a	6750(30)	5663(5)	4655(18)	96(3)
H49b	6440(40)	5224(10)	5106(5)	96(3)
H49c	5434(12)	5365(15)	4553(15)	96(3)
H50	1853(6)	7076(2)	6681(3)	54.8(18)
H51	-195(6)	6799(3)	6390(3)	69(2)
H53	-50(7)	7325(3)	4799(4)	77(2)

H54	1993(6)	7579(3)	5118(3)	62(2)
H55a	-1717(7)	6466(11)	5190(30)	135(5)
H55b	-2176(19)	6850(30)	5654(8)	135(5)
H55c	-2120(20)	7087(18)	5030(20)	135(5)
H59	3394(5)	6346(2)	6863(2)	35.8(14)
H57a	4270(19)	7115(17)	8860(30)	176(6)
H57b	4627(12)	6478(19)	8880(30)	176(6)
H57c	4340(20)	6780(40)	9440(4)	176(6)
H60a	-670(110)	10956(14)	5070(30)	292(11)
H60b	-830(100)	11320(50)	5610(20)	292(11)
H60c	300(20)	11430(40)	5290(50)	292(11)

References

[S1] Dulière , E.; Devillers , M.; Marchand-Brynaert, J. *Organometallics*, **2003**, *22*, 804–811

[S2] Pearson, P.; Bond, A. M.; Deacon, G. B.; Forsyth, C.; Spiccia, L. *Inorg. Chem. Acta*, **2008**, *361*, 601–612.

[S3] Duan, L.; Xu, Y.; Gorlov, M.; Tong, L.; Andersson, S.; Sun, L.; *Chem. Eur. J.*, **2010**, *16*, 4659–4668.

[S4] Rabten, W.; Kärkäs, M. D.; Åkermark, T.; Chen, H.; Liao, R.-Z.; Tinnis, F.; Sun, J.; Siegbahn, P. E. M.; Andersson, P. G.; Åkermark, B. *Inorg. Chem.*, **2015**, *54*, 4611–4620.

[S5] Chiriac, C. I.; Onciu, M.; Tanasa, F. *Designed Monomers and Polymers*, **2004**, *4*, 331–335.

[S6] Sander, A. C.; Maji, S.; Francàs, L.; Böhnisch, T.; Dechert, S.; Llobet, A.; Meyer, F. *ChemSusChem*, **2015**, *10*, 1697–1702.

[S7] Laviron, E. *J. Electroanal. Chem*., **1979**, *101*, 19–28.

[S8] Laviron, E. *J. Electroanal. Chem*., **1972**, *35*, 333–342.

[S9] E_i is the vertex potential (V).

[S10] Gao, Y.; Åkermark, T.; Liu, J.; Sun, L.; Åkermark, B. *J. Am. Chem. Soc*. **2009**, *131*, 8726–8727.

[S11] Rabten, W.; Kärkäs, M. D.; Åkermark, T.; Chen, H.; Liao, R.-Z.; Tinnis, F.; Sun, J.; Siegbahn, P. E. M.; Andersson, P. G.; Åkermark, B. *Inorg. Chem.*, **2015**, *54*, 4611–4620.

[S12] Dolomanov, O. V.; Bourhis, L. J.; Gildea, R. J.; Howard, J. A. K.; Puschmann, H. *J. Appl. Cryst*., **2009**, *42*, 339–341.

[S13] Sheldrick, G. M. *Acta Cryst*., **2015**, *A71*, 3–8.

[S14] Bourhis, L. J.; Dolomanov, O. V.; Gildea, R. J.; Howard, J. A. K.; Puschmann, H. *Acta Cryst*., **2015**, *A71*, 59–75.